1-25-2018

The Ecosystem Baseline for Particle Flux in the Northern Gulf of Mexico

S.L.C. Giering
University of California, Santa Barbara

Beizhan Yan
Lamont-Doherty Earth Observatory of Columbia University, yanbz@ldeo.columbia.edu

Vernon Asper
University of Southern Mississippi, vernon.asper@usm.edu

Arne-R. Diercks
University of Southern Mississippi, Arne.Diercks@usm.edu

Jeff Chanton
Florida State University, jchanton@fsu.edu

See next page for additional authors

ELEMENTA
Science of the Anthropocene

Giering, SLC, et al. 2018 The ecosystem baseline for particle flux in the Northern Gulf of Mexico. *Elem Sci Anth,* 6: 6.
DOI: https://doi.org/10.1525/elementa.264

RESEARCH ARTICLE

The ecosystem baseline for particle flux in the Northern Gulf of Mexico

S.L.C. Giering[*,†], B. Yan[‡], J. Sweet[*], V. Asper[§], A. Diercks[§], J.P. Chanton[‖], M. Pitiranggon[‡] and U. Passow[*]

Response management and damage assessment during and after environmental disasters such as the Deepwater Horizon (DWH) oil spill require an ecological baseline and a solid understanding of the main drivers of the ecosystem. During the DWH event, a large fraction of the spilled oil was transported to depth via sinking marine snow, a routing of spilled oil unexpected to emergency response planners. Because baseline knowledge of particle export in the Northern Gulf of Mexico and how it varies spatially and temporally was limited, we conducted a detailed assessment of the potential drivers of deep (~1400 m depth) particle fluxes during 2012–2016 using sediment traps at three contrasting sites in the Northern Gulf of Mexico: near the DWH site, at an active natural oil seep site, and at a site considered typical for background conditions. The DWH site, located ~70 km from the Mississippi River Delta, showed flux patterns that were strongly linked to the Mississippi nitrogen discharge and an annual subsequent surface bloom. Fluxes carried clear signals of combustion products, which likely originated from pyrogenic sources that were transported offshore via the Mississippi plume. The seep and reference sites were more strongly influenced by the open Gulf of Mexico, did not show a clear seasonal flux pattern, and their overall sedimentation rates were lower than those at the DWH site. At the seep site, based on polycyclic aromatic hydrocarbon data, we observed indications of three different pathways for "natural" oiled-snow sedimentation: scavenging by sinking particles at depth, weathering at the surface before incorporation into sinking particles, and entry into the food web and subsequent sinking in form of detritus. Overall, sedimentation rates at the three sites were markedly different in quality and quantity owing to varying degrees of riverine and oceanic influences, including natural seepage and contamination by combustion products.

Keywords: Deepwater Horizon; Gulf of Mexico; marine oil snow; sedimentation; particle flux; polycyclic aromatic hydrocarbon

1. Introduction

The Northern Gulf of Mexico is a very dynamic and high-contrast ecosystem. In the oligotrophic offshore regions, phytoplankton are nutrient-limited and primary production is low. Near the coast, the Mississippi River supplies nutrients (primarily nitrate) in such quantities that large regions become anoxic during summer (Turner et al., 2008). The Mississippi also carries large amounts of fine, suspended sediment, which settles near the Mississippi Delta and dominates the seafloor sediment there (Balsam and Beeson, 2003; Ellwood et al., 2006). This eutrophic river plume is advected by the strong currents in the Gulf of Mexico depending on the wind conditions and the position of the loop current (Walker, 1996; Walker et al., 2005; Schiller et al., 2011), and can at times be detected as far south as the Florida Straight (Hu et al., 2005; Schiller and Kourafalou, 2014). The complex interaction between different waters (with differing nutrient and trophic states) and highly variable currents leads to a very heterogeneous and dynamic system. This complexity likely affects particles that sink from the surface, ultimately supply carbon to the deep sea community, and play an important role in the carbon cycle. However, to date, knowledge of this important pathway and how it varies spatially and temporally in the Northern Gulf of Mexico is very limited (Davies et al., 2010; Mienis et al., 2012; Prouty et al., 2016). This limitation became especially apparent during the Deep Water Horizon (DWH) oil spill when it was realized that sinking particles were concentrating and transporting large amounts of oil to depth (Passow et al., 2012).

* University of California, Santa Barbara, California, US
† National Oceanography Centre, Southampton, UK
‡ Lamont-Doherty Earth Observatory of Columbia University, Palisades, New York, US
§ University of Southern Mississippi, Stennis Space Center, Mississippi, US
‖ Florida State University, Tallahassee, Florida, US
Corresponding author: U. Passow (uta.passow@lifesci.ucsb.edu)

The Macondo DWH oil spill (from 20 April 2010 to 15 July 2010) was the second largest oil spill in history and unprecedented for several reasons, one of them being the observation that large amounts of the oil were incorporated into marine snow and deposited on the seafloor (Passow et al., 2012; Daly et al., 2016). This marine oil snow sedimentation and flocculent accumulation (MOSSFA) event was an unexpected fate for a large amount of the spilled oil: the estimates that 5–10% or even 15% of the released oil was transported to the sea floor via MOSSFA (Valentine et al., 2014; Chanton et al., 2015; Stout et al., 2017) are almost certainly too low (Passow and Ziervogel, 2016).

1.1. Marine snow, aggregation and flux

Marine snow originates in the surface ocean and forms via the interaction of phytoplankton, zooplankton, bacteria and lithogenic matter. Several of the organisms involved have unique elemental compositions and can produce minerals with high excess density (compared to seawater). For example, phytoplanktonic coccolithophores and zooplanktonic foraminifera and pteropods produce shells that contain calcium carbonate ($CaCO_3$). Phytoplanktonic diatoms or radiolarians produce cell walls that contain the mineral biogenic silica ($bSiO_2$). Most other planktonic organisms, such as bacteria and most zooplankton are composed primarily of organic compounds. In the open ocean, the composition of this marine snow is determined by the abundance and species composition of the plankton, with a higher abundance of coccolithophores causing higher $CaCO_3$ concentrations in marine snow, whilst a higher abundance of diatoms causes a higher proportion of $bSiO_2$. In near-shelf systems or areas with high dust inputs, terrestrial matter (in particular 'lithogenic matter') can make up a significant fraction of marine snow.

Marine snow particles can sink at a variety of speeds ranging from only few cm per day to several hundreds of meters per day (Turner, 2002; Alonso-González et al., 2010; McDonnell and Buesseler, 2010), but are commonly thought to sink at an average of 10–150 m d^{-1} (McDonnell and Buesseler, 2010; Villa-Alfageme et al., 2016). Depending on the sinking speed of an individual aggregate, marine snow can be transported horizontally over several hundreds of kilometers in regions with strong currents (Siegel and Deuser, 1997). The location where an aggregate eventually lands on the seafloor could thus differ markedly from the location where it was formed. Whilst sinking through the water column, marine snow is reworked and much of it is lost due to remineralization and grazing, leading to a rapid decline in flux with depth (Martin et al., 1987; Buesseler et al., 2008). On the other hand, aggregates also scavenge dissolved or non-sinking particles during sinking, which alters their composition (Passow and De La Rocha, 2006; De La Rocha and Passow, 2007).

1.2. Transport of contaminants by marine snow

Marine snow is known to transport contaminants including oil residues to the seafloor (Paasivirta et al., 1982; Broman et al., 1987; Baker et al., 1990; Lipiatou et al., 1993; Lee and Page, 1997). Hydrophobic organic contaminants can associate with particulate and dissolved organic carbons (Hites and Eisenreich, 1987; Wang and Zhang, 2014), which may lead to their incorporation into marine snow and subsequent settling to the seafloor. Oil residues in the form of polycyclic aromatic hydrocarbons (PAHs) have been found in sediment traps in lakes (Baker et al., 1991), coastal regions (Paasivirta et al., 1982; Broman et al., 1987), and the deep sea (deeper than 1000 m depth; Lipiatou et al., 1993; Yan et al., 2016).

After DWH, high amounts of petrogenic PAHs were found in sediment traps even months after the well was closed (Yan et al., 2016). To fully assess when the ecosystem and fluxes have returned to baseline levels after a spill, the background concentrations need to be known. Meeting this need is not trivial, because sinking aggregates can contain PAHs from a variety of sources, including naturally occurring PAHs that are petrogenic (petroleum-derived; e.g., from natural seeps) and pyrogenic (combustion-derived; e.g., from wildfires) as well as anthropogenic petrogenic (e.g., engine oils and chronic oil leakage) and pyrogenic (e.g., automobile, industrial and power plant emissions). For the Gulf of Mexico, a pre-spill baseline of measured marine snow fluxes does not exist, which has two consequences. Firstly, it is not known at what time point sedimentation rates return to usual conditions (both in terms of magnitude and PAH contents) – in other words, damage assessment is hampered. Secondly, a detailed understanding of seasonal and spatial variability in 'background' fluxes in the Gulf of Mexico is necessary for future oil spill response management when evaluating the potential for MOSSFA formation.

The purpose of this study was to identify what determines the magnitude, composition and temporal variability of deep (>1000 m depth) particle fluxes in the Northern Gulf of Mexico. We hypothesized that deep fluxes are strongly influenced by the Mississippi River discharge and the strong currents and that they normally do not carry large amounts of fossil carbon contaminants. We here present marine snow flux data collected using sediment traps from three sites in the Northern Gulf of Mexico from 2012 to 2016. Analysis of oil components in the flux offers additional insights into different aggregate transport pathways. These data provide a post-DWH particle flux baseline and novel insights into what drives particle export spatially and temporally in this region.

2. Methods

2.1. Deployment sites

Three long-term monitoring sites were chosen in the Northern Gulf of Mexico (**Table 1** and **Figure 1**). The first site – the 'DWH site' (R/V *Oceanus* Site 26; 28°40'N, 88°21.6'W; 1660 m deep) – is located in the Mississippi Canyon lease area in close proximity (~5 km) to the DWH blowout location and near the main Mississippi River Delta (~70 km southeast). This site, also referred to as 'OC26' in the literature, is monitored frequently and is the location of the sediment trap deployed after DWH (Yan et al., 2016). The second site – the 'Seep site' (27°22.5'N, 90°30.6'W; 1380 m deep) – is located in

Green Canyon lease block GC600 within a very active natural oil seep area (Roberts et al., 2010), which often has extensive oil slicks at the surface ocean (Macdonald et al., 1993; MacDonald et al., 2002). This high seepage activity has recently been linked to elevated surface chlorophyll *a* concentrations (D'souza et al., 2016). Our third site – the 'Reference site' (27°31.5 N, 89°42.6 W; 1160 m deep) – will be used as an index for typical background conditions, although sediment analysis suggests that this site is also at times exposed to oil from natural seeps (Fisher et al., 2014). This site is located in Atwater Valley lease block AT357 at the largest currently known deepwater coral assemblage in the Gulf of Mexico (Doughty et al., 2014). Both Seep and Reference sites were not visibly impacted by DWH (Fisher et al., 2014). Temperatures at the traps were between 4.2 and 4.5°C at all sites. The average current speeds (±SD) ~45 m below the trap (~75 m above the bottom) were < 3.8 ± 2.0 cm s^{-1} (n = 19664) and < 4.9 ± 3.0 cm s^{-1} (n = 9645) at the DWH and Seep site, respectively (Diercks et al., 2017). Sediment trap data are generally considered reliable as long as current velocities remain under 10 cm s^{-1} (Gardner, 1980).

2.2. Trap deployments

Sediment traps (*Parflux Mark 78H*, McLane Research Laboratories and *Kiel Trap*, K.U.M. Umwelt- und Meerestechnik Kiel GmbH) have been deployed since April 2012, collecting sediment fluxes at 120 m above the sea bed (water depths of 1540 m, 1260 m and 1040 m at the DWH, Seep and Reference sites, respectively). Here we present data until September 2016. All three time-series traps had catchment areas of 0.5 m^2, covered with a hexagonal lattice grid baffle that reduces washout. The multi-bottle turntables allowed for the collection of 13–21 time-series samples per deployment period (~1 year), collecting for 11–28 days each (**Table 1**). After each of the collection periods, traps were recovered and re-deployed within a few days to generate a continuous time series.

The DWH site trap was successfully deployed for the entire period. However, towards the end of several deployment periods, the trap funnel clogged and the subsequent samples were lost (26 June–15 September 2014, 29 March–15 September 2015, and 19 February–12 September 2016). This clogging was likely caused by high export rates, such that the average annual fluxes presented for the DWH site are likely underestimates

Table 1: Deployment details of the three sediment traps. DOI: https://doi.org/10.1525/elementa.264.t1

Site	Position	Trap type (number of cups)	Deployment period	Collection period per cup (d)	Water depth (m)	Deployment depth (m)
DWH	28°40.8 N 88°21.7 W	McLane (21)	28 June 2012 to 12 September 2016	16 or 18	1660	1540
Seep	27°22.5 N 90°30.7 W	McLane (13)	16 April 2012 to 15 April 2016	11, 18, 24, 27, 28	1380	1260
Reference	27°31.5 N 89°42.6 W	Kiel-trap (20)	16 April 2012 to 25 April 2016	17 or 18	1160	1040

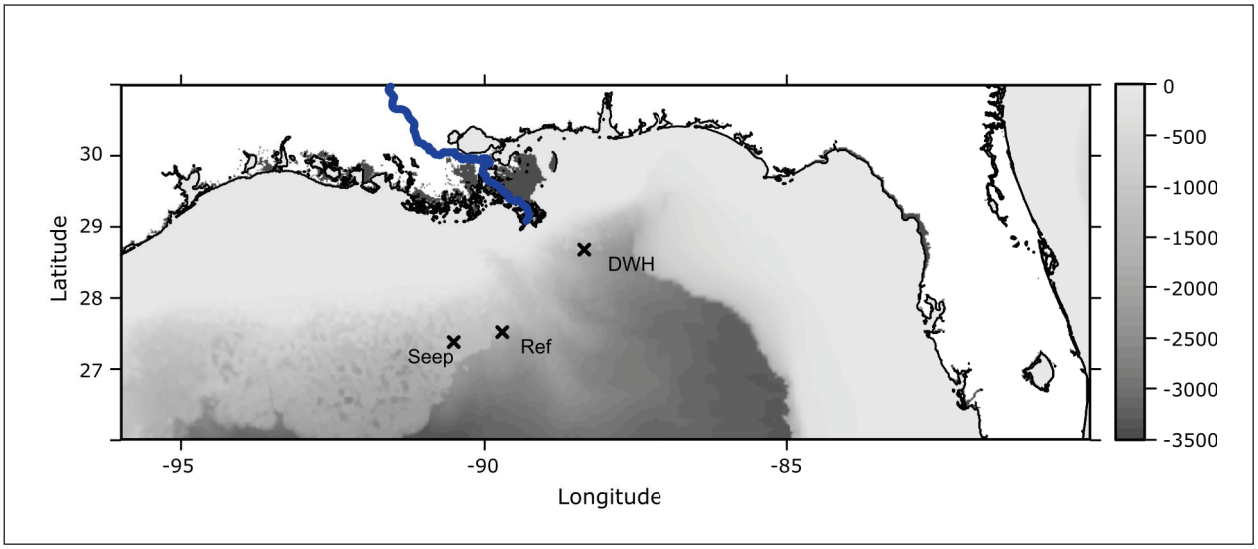

Figure 1: Map of the sampling area with locations of the three sediment trap sites. The three trap sites – Deepwater Horizon (DWH), Seep, and Reference (Ref) sites – in the Northern Gulf of Mexico are overlaid on the seabed topography. Scale bar indicates depth in meters. Blue line represents the Mississippi River. DOI: https://doi.org/10.1525/elementa.264.f1

(see Section 4.1). The trap at the Seep site sampled successfully for the entirety of all deployment periods. The trap at the Reference site sampled successfully between April 2012 and January 2015. However, during the 2014–2015 deployment a mechanical failure occurred after 22 August 2015 (during cup 7 out of 13) and the remaining samples were lost. The trap was serviced before redeployment for the next year but did not rotate, so that no samples were collected during the 2015–2016 deployment.

2.2.1. Trap sample processing

Prior to deployment, sample bottles were filled with filtered seawater to which NaCl (Pro analysis, Fisher) was added to a final salinity of ~40 and the preservative $HgCl_2$ to a final concentration of ~0.14%. Using $HgCl_2$ rather than buffered formalin allows for C-isotopic determinations. Upon retrieval, cups were stored dark and cold (4°C) until processing. First, cups were gently mixed and, after the material was allowed to resettle for 7 days, the supernatant was sampled for pH, salinity and nutrients. Lower pH, salinity or nutrient concentrations than expected indicates a preservation anomaly or wash out. Preservation was as expected in all cups and no signs of degradation were observed. Some cups with high sedimentation fluxes showed signs of $bSiO_2$ dissolution, but potential dissolution (estimated by assuming that excess $Si(OH)_4$ in the supernatant compared to ambient water originated from dissolution) was equivalent to < 10% of measured $bSiO_2$ flux. We did not correct for potential dissolution, but note that high $bSiO_2$ fluxes are potentially slightly underestimated (by < 10%).

Sample material was split repeatedly into five or ten subsamples, using a sample splitter (*WSD–10*, McLane Research Laboratories). During splitting artificial seawater was used for rinsing. The splitting introduces an error of about 3–5% in terms of mass flux (unpublished data; Honjo et al., 2008). Individual splits were used for different analyses. Appropriate split size for any biochemical measurement depended on the total amount of material collected per cup and on the method, varying between 1/10 and 1/2,500. Trap material was not screened or routinely picked before filtration, as we consider moults, carcasses, large shells or scales to be part of the flux. Detailed notes for each cup and split can be found in the raw data. (DOI: https://doi.org/10.7266/N7F47M6M, DOI: https://doi.org/10.7266/N79C6VHB, DOI: https://doi.org/10.7266/N7XK8CZS, DOI: https://doi.org/10.7266/N78W3BQJ, DOI: https://doi.org/10.7266/N7H993KF, DOI: https://doi.org/10.7266/N7CJ8BVQ, DOI: https://doi.org/10.7266/N7416VD0, DOI: https://doi.org/10.7266/N7PN93PS, DOI: https://doi.org/10.7266/N7JW8BXM, DOI: https://doi.org/10.7266/N7CR5RQT, DOI: https://doi.org/10.7266/N7VT1QGS, DOI: https://doi.org/10.7266/N7BR8QKF and DOI: https://doi.org/10.7266/N71C1V8T)

2.3. Flux component analyses

Total mass flux was calculated from dry weight (DW): quadruplicate splits were filtered onto pre-weighed (AE160, Mettler Toledo) and pre-combusted (450°C for 4–6 hours) GF/F filters (25-mm diameter, nominal pore size 0.7 μm, Whatman), briefly rinsed with Milli-Q water, dried at 60°C (4–6 hours), and weighed. DW was defined as the difference between dried and pre-weighed filter. The filters were then used to determine particular organic carbon (POC), particulate organic nitrogen (PON) and particulate inorganic carbon. Duplicate filters were fumed with 10% HCl to remove inorganic carbon. All filters were then analyzed using a CHN elemental analyzer (CEC 44OHA; Control Equipment, now Exeter Analytical). Particulate inorganic carbon was defined as the difference of the acidified and non-acidified particulate carbon (Shipe and Brzezinski, 2003). Calcite ($CaCO_3$) content was calculated from particular inorganic carbon by assuming a molecular weight of 100. For some traps we also analyzed for combustible and non-combustible matter by combustion (450°C for 4–6 hours) and reweighing a third time, though the data are not presented here. Biogenic silica ($bSiO_2$) was analyzed by filtering splits onto 0.6-μm polycarbonate filters (47-mm diameter, Millipore) (DeMaster, 1981; Mortlock and Froelich, 1989). Filters were hydrolyzed with Na_2CO_3, running a 0.5 to 5 hour time series, and analyzed colourimetrically (Shipe and Brzezinski, 2001). The change in the slope of dissolution rate indicates the shift from $bSiO_2$ to lithogenic silica dissolution and was used to determine $bSiO_2$ concentration. $bSiO_2$ was assumed to have a molar mass of 67.

The concentration of lithogenic material (Lith) was calculated as:

$$Lith = DW - \left(CaCO_3 + bSiO_2 + 2.2\,POC\right) \qquad (1)$$

POC was converted to total organic matter using the commonly used conversion factor of 2.2 based on reported conversion factors ranging between 1.9 and 2.3 (Honjo, 1980; Tsunogai, 1987; Klaas and Archer, 2002; Boyd and Trull, 2007; Salter et al., 2010).

For analysis of transparent exopolymer particles (TEP), a series of three to five sub-splits (ranging between 1/2,500 and 1/12,500 or 1/12,500 and 1/62,500, depending on the TEP concentration and sample volume) were filtered in triplicate onto 0.4-μm polycarbonate filters (25-mm diameter, Whatman) as described in Passow and Alldredge, (1995), and corrected using unstained and blank filters as detailed in Passow et al. (2001). The slope of the linear relationship was used to calculate TEP concentration. Xanthan gum was used to calibrate the Alcian Blue solution, with TEP expressed as Xanthan gum equivalent.

Fluxes for each component (F_x) were calculated as:

$$F_x = \frac{\bar{m}_x}{A\,t} \qquad (2)$$

where $\bar{m}_x$ is the average mass per cup (after normalizing for splitting), x is the component, A is the trap area (0.5 m^2), and t is the collection period for each cup (in days). Where multiple replicates were analyzed, the standard deviation (SD) is stated. No SD is given for TEP and $bSiO_2$ flux because these values were based on the slope of a linear regression of different sample concentrations.

2.4. Hydrocarbon concentration and composition

Flux and composition of hydrocarbons (C_{16}–C_{36} *n*-alkanes, selected polycyclic hydrocarbons, pristane, phytane and hopanes) were measured for the period of April 2012–April 2013 for the Seep and Reference sites, and for the period between July and September 2012 at the DWH site. Analysis for hydrocarbons and olefins was carried out as described by Yan et al. (2016). A full list of all measured compounds can be found in the supplementary material (Table S1). ΣPAH fluxes were calculated by multiplying ΣPAH concentrations with DW flux. To distinguish between different sources, we used the sample indices and criteria used by Yan et al. (2016) to identify the hydrocarbon sources in marine snow after the DWH spill.

The carbon preference index (CPI) refers to the ratio of alkanes with an odd number of carbon atoms over those with an even number of carbon atoms. Higher (terrestrial) plants have been shown to produce a higher proportion of odd than even hydrocarbons with a CPI of ≥ 5. For phytoplankton, data are not conclusive, though they generally tend to produce shorter alkanes (C_n with n < 20) (Volkman et al., 1998). Fossil fuels have a CPI of ~1. We calculated the CPI index for alkanes between C_{24} to C_{36} following:

$$CPI = 0.5 \times \left(\frac{\sum \{C_{24}, C_{35}\}_{odd}}{\sum \{C_{24}, C_{35}\}_{even}} + \frac{\sum \{C_{25}, C_{36}\}_{odd}}{\sum \{C_{25}, C_{36}\}_{even}} \right) \quad (3)$$

As boundary values, we used the values applied by Yan et al. (2016), which indicate that samples with a CPI < 1.6 are dominated by crude-oil alkanes.

To distinguish between pyrogenic (combustion) and petrogenic (crude oil) sources, we used two indices. Pyrene is thermodynamically more stable than its homologue fluoranthene. As a consequence, high-temperature processes such as combustion lead to a higher ratio of the unstable to the stable homologue. A ratio of fluoranthene to fluoranthene + pyrene (Fl/(Fl+Py)) > 0.5 (i.e., a high ratio of unstable to stable homologue) suggests a dominance of pyrogenic PAH sources, while a Fl/(Fl+Py) < 0.4 suggests a dominance of petrogenic PAH sources (Budzinski et al., 1997; Yan et al., 2016). We also used the index $C_0/(C_0+C_1)$, which is the ratio of parent phenanthrene to phenanthrene plus its monomethyl homologues (2-methylphenanthrene, 1-methylphenanthrene, 3-methylphenanthrene, and 4-methylphenanthrene). Methylation occurs during the formation of PAHs, and crude oils are dominated by alkylated PAHs (Blumer, 1976). At high temperatures (i.e., combustion) the less stable alkyl group is lost, leading to low levels of methylation in combustion products. Following Yan et al. (2016), $C_0/(C_0+C_1) \leq 0.5$ was interpreted as a dominance of PAHs from crude oil.

Finally, we calculated the average chain length (ACL) of n-alkanes as:

$$ACL = \frac{\sum i \times c_i}{\sum c_i} \quad (4)$$

where C_i is the concentration of the n-alkane with *i* number of C atoms (Poynter and Eglinton, 1990).

To categorize the dominant hydrocarbon sources, we used overall PAH concentration, ACL, the three indices (CPI, Fl/(Fl+Py), $C_0/(C_0+C_1)$, and isotopic composition. In unclear cases, a final judgment was influenced by the occurrence and concentration of individual PAHs and their most likely source (for example, 5–6 ringed and methylated PAHs indicating pyrogenic and petrogenic sources, respectively).

2.5. Isotopic analysis

Prior to isotopic analysis samples were dried, ground, treated with 10% HCl to remove carbonates, rinsed and freeze-dried. Samples for Δ^{14}C-POC analysis were combusted in quartz tubes for 18 hours at 850°C, and purified CO_2 was prepared as graphite targets and analyzed by accelerator mass spectrometry (Vogel et al., 1984). Values are reported according to the Δ notation put forth in Stuiver and Polach (1977). The Δ notation normalizes the radiocarbon content of a sample to a nominal δ^{13}C value (–25‰) and the collection time. The scale is linear and starts at –1000‰ when a sample has essentially 0% modern carbon, which would represent petroleum residue (McNichol and Aluwihare, 2007). Analytical reproducibility was on the order of 3‰. For details see Chanton et al. (2017).

2.6. Primary production, discharge data and topography

Primary production (PP) estimates were based on satellite data and the Vertically Generalized Production Model (VGPM) which estimates light-dependent, depth-resolved carbon fixation (Behrenfeld and Falkowski, 1997). Model results were obtained from the Ocean Productivity site (http://www.science.oregonstate.edu/ocean.productivity/). PP was calculated as the median for 8-day composites for 0.5-degree boxes around the study sites from January 2010 to November 2016.

Discharge and nitrate + nitrite (N) concentrations of the Mississippi River were obtained from USGS (https://waterdata.usgs.gov/) for the time period between 1 January 2010 and 9 September 2011 at Francisville, LA (site ID USGS 07373420; samples approximately every 2 weeks), and for the time period between 9 September 2011 and 31 December 2016 at Baton Rouge, LA (site ID USGS 07374000; high resolution sampling with several samples daily). The two sites are < 50 km apart from each other, and a comparison of discharge and nutrient concentrations at the two sites for 2012 showed that the stream conditions varied little between the two sites.

The topography of the study area was downloaded at 1-minute resolution from NOAA using the getNOAA.bathy function in the R package marmap (Amante and Eakin, 2009).

2.7. Statistics

Seasonal patterns in POC flux and PP at the three sites were determined with a smoothing function that uses cyclic cubic regression splines from the mgvc package

in R. As these patterns are for illustrative purposes, no further statistics were carried out. To calculate annual fluxes, measured fluxes were estimated for every day during the study periods using linear interpolation between the mid-points of each cup-sampling period. The running sum for 365 consecutive days was calculated, and average and SD were calculated for all running sums (n = 950, 1077 and 477 at the DWH, Seep and Reference sites, respectively). A higher number of observations n indicates a longer time series. The relationship between flux components was tested using simple linear regression. As the data were right-skewed and contained zeros; linear regression was performed on both untransformed and root-cube transformed data. The level of statistical significance was the same for both regressions (transformed versus untransformed), and the R^2 values were similar (slightly higher for cube-root transformation in 17 out of 21 regressions). As the interpretation is not compromised, we state the results of the untransformed regressions here.

Hydrocarbon composition was analyzed using multivariate ordination analysis from the *vegan* package in R (R Core Team, 2015; Oksanen et al., 2016). In addition to our 2012–2013 samples, we included the sediment trap samples collected at the DWH site for the year following the spill (Yan et al., 2016).

We used 40 groups of hydrocarbons (Table S1) to calculate dissimilarities between samples using non-metric multidimensional scaling (NMDS). We applied Bray-Curtis dissimilarities, two dimensions, and Wisconsin double standardization, which reduces the influence of samples with high concentrations. The stress of the solution was low (stress = 0.12). The solution was centered and scaled so that one unit corresponds to halving the similarity between two samples. The solution was rotated so that the first axis approximates the gradient in ΣPAH concentrations, and the second axis approximates the shift from petrogenic to pyrogenic sources based on methylation and number of aromatic rings. Detailed explanations of the functions can be found in the *metaMDS* help package (Oksanen et al., 2016).

The differences between the three sites (DWH, Seep and Reference sites) and between the five periods identified for the Seep site (see Section 3.4) – referred to as *a priori* groups – were tested with non-parametric multivariate analysis of variance (PERMANOVA) (Anderson, 2001). Dissimilarity indices were calculated after transformation (as described above) using the vegdist function, whose results are identical to the *metaMDS* function but differ in its output format. Significant differences between *a priori* groups were tested using the *adonis* function with 999 random permutations. Significant differences in group centroids calculated using adonis can be caused either by differences in the centroid locations or by differences in data spread ('dispersion') (Anderson, 2006). We tested for differences in dispersion using the function *betadisper* and the ANOVA-like function *permutes* (with 999 random permutations) as well as Tukey's test. Differences in dispersion never compromised the results of diagnosed differences in centroid location.

3. Results

3.1. Primary production

The DWH site was by far the most productive site. Located just offshore of the main Mississippi outlet, it showed the highest surface primary production (PP) rates of all three sites (mean ± SD of 1.2 ± 1.2 g m^{-2} d^{-1}, n = 223) with a maximum of 6.7 g m^{-2} d^{-1} (**Figure 2a**). PP was lowest in autumn (September–October). The climatology suggests that the DWH site experiences an annual winter bloom consistently around February. During summer, the PP is more variable but suggests peak values around July, though this bloom does not appear to occur every year (**Figure 2a**).

The Seep and Reference sites show very similar annual PP rates (mean ± SD of 0.4 ± 0.2 g m^{-2} d^{-1} at both the Seep and Reference sites, n = 223) and maximum PP of < 1 g m^{-2} d^{-1} (**Figure 2b, c**). Similar to the DWH site, both sites consistently showed lowest PP values in September–October and a winter bloom in February. However, there was no obvious summer bloom (though occasionally slightly elevated PP rates were observed during June–July) and overall PP rates were much lower than at the DWH site.

3.2. Flux rates and composition in the Northern Gulf of Mexico

At the DWH site, fluxes of all components, with the exception of $CaCO_3$, were higher compared to the other two sites (**Figure 3**). Total matter fluxes indicated the transport of an annual mean ± SD of 175 ± 52 g DW m^{-2} $year^{-1}$ at the DWH site, with average daily fluxes ranging from 99 to 2,228 mg DW m^{-2} d^{-1} (**Table 2**). In any one cup, the bulk of these fluxes was comprised of lithogenic material (mean of 69 ± 7%, n = 56), with organic matter (2.2 × POC), $bSiO_2$, and $CaCO_3$ making up roughly the same contribution (9 ± 3%, 9 ± 2% and 12 ± 8%, respectively; **Table 2**). POC fluxes averaged 17 ± 13 mg C m^{-2} d^{-1} (n = 58, range of 5–64 mg C m^{-2} d^{-1}; **Figure 2d**, **Table 2**). Annual flux rates are likely underestimates, as peak fluxes were likely missed due to trap clogging (see Section 4.1).

At the Reference site, fluxes of all components were lowest (**Table 2** and **Figure 3**). Average annual total matter fluxes were approximately 20% of the fluxes observed at the DWH site. Organic matter, $bSiO_2$ and lithogenic annual fluxes were 25%, 16% and 15% of the respective fluxes at the DWH site. The exception was $CaCO_3$, which was 46% of the flux observed at the DWH site. This exception is also reflected in the higher percentage of $CaCO_3$ in fluxes in each cup (29 ± 31%, n = 46) compared to that of the DWH site (12 ± 8%, n = 58). Similar to the DWH site, lithogenic matter made up the bulk of the fluxes in any one cup (mean of 50 ± 23%, n = 46), albeit to a lesser extent than at the DWH site and with a more variable contribution. $bSiO_2$ contributed 9 ± 4% (n = 46) of the flux. Average annual total matter fluxes were 32 ± 5 g DW m^{-2} d^{-1} at the Reference site, with fluxes in each cup ranging from 3 to 639 mg DW m^{-2} d^{-1} (**Table 2**). POC fluxes averaged 6 ± 5 mg C m^{-2} d^{-1} (range: 1–25 mg C m^{-2} d^{-1}).

The Seep site appeared to be in between the DWH and Reference sites in terms of absolute fluxes and flux

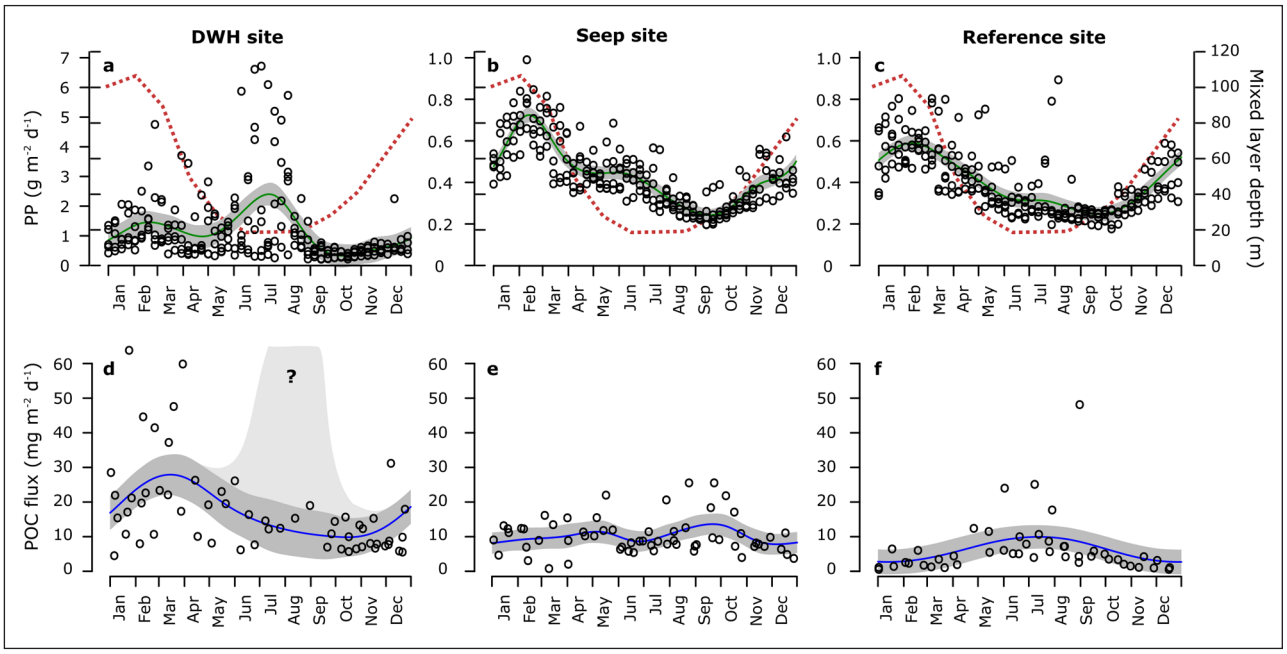

Figure 2: Seasonal patterns of primary production, mixed layer depth, and POC fluxes at the three sites. Seasonal pattern of **(a–c)** integrated primary production (PP) and mixed layer depth, and **(d–f)** POC fluxes at the DWH site (left), the Seep site (middle) and the Reference site (right) during 2012–2016. (a–c) Integrated primary production (PP, open circles) calculated from satellite data using the VGPM model in 8-day intervals. The seasonal pattern is captured using a cyclic spline smoother (green line), with the grey area showing the 95% confidence intervals. Monthly climatology of the mixed layer is shown as a dotted red line according to Muller-Karger et al. (2015). (d–f) POC flux at ~1400 m depth during 2012–2016 measured using sediment traps (open circles). The seasonal pattern in captured using a cyclic spline smoother (blue line), with the grey area showing the 95% confidence intervals. For the DWH site (d), clogging of the traps meant no reliable estimate of peak fluxes. The uncertainty in peak fluxes is indicated with the light grey area and marked with a question mark. DOI: https://doi.org/10.1525/elementa.264.f2

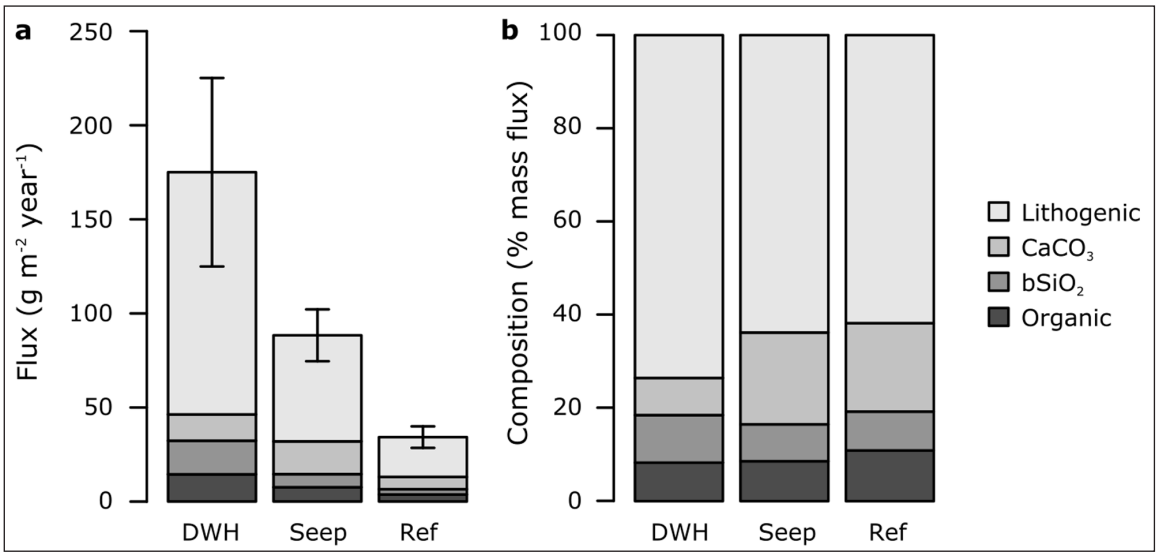

Figure 3: Annual averages of flux and flux composition at the three sites. (a) Annual flux averages at the Deepwater Horizon (DWH), Seep and Reference (Ref) sites, calculated using a running mean on daily fluxes. Daily fluxes were calculated based on 58, 60 and 46 samples, respectively for the three sites. The error bars show SD of all computed means of daily fluxes (n = 950, 1077 and 477 at the DWH, Seep and Reference sites, respectively). Note that DWH site fluxes are likely underestimates because of trap clogging during periods of high PP. **(b)** Flux composition as percentages of total mass flux, with flux components colored according to the inset legend. Organic refers to total particulate organic matter calculated as 2.2 × POC (see text). DOI: https://doi.org/10.1525/elementa.264.f3

composition (**Table 2**), though it is farthest to the west (**Figure 1**). Average annual total mass flux was 85 ± 15 g DW m^{-2} d^{-1}, with fluxes in each cup ranging from 27 to 643 mg DW m^{-2} d^{-1} (**Table 2**). Annual fluxes at the Seep site are thus ~50% of the fluxes at the DWH site during this time frame, but 2.5 times higher than those at the Reference site. In terms of average annual fluxes, lithogenic matter made up 60 ± 15% (n = 60) of the flux in any one cup, a contribution that is lower than that at the DWH site (69 ± 7%, n = 56) but higher than at the Reference site (50 ± 23%, n = 46). The contribution of biogenic minerals ($bSiO_2$ and $CaCO_3$) to flux was similar at the Seep and Reference sites ($bSiO_2$: 9 ± 4% at both sites; $CaCO_3$: 21 ± 17% and 29 ± 31%, respectively). Daily POC fluxes averaged 10 ± 5 mg C m^{-2} d^{-1} (range: 1–26 mg C m^{-2} d^{-1}), and thus half of those observed at the DWH site but overall higher than those at the Reference site (**Table 2**).

Most flux compounds were significantly correlated with each other (**Table 3**). The strongest correlation was observed between total mass flux and lithogenic flux (R^2 = 0.94, $p < 0.01$, n = 162), POC and PON (R^2 = 0.94, $p < 0.01$, n = 166), and total mass flux and POC (R^2 = 0.77, $p < 0.01$, n = 166). No correlation was observed between $CaCO_3$ and any of the other compounds. The C:N ratios of sinking organic particles (mean of 9.2 ± 2.1 mol mol^{-1}, n = 165) were in the range of those from traps at this depth (Schneider et al., 2003), with higher C:N ratios (9.9 ± 2.1 mol mol^{-1}, n = 58) at the near-shore DWH site compared to the two more off-shore stations (8.9 ± 1.2 mol mol^{-1}, n = 61, at the Seep site and 8.7 ± 2.6 mol mol^{-1}, n = 46, at the Reference site).

All data are available at https://data.gulfresearchinitiative.org/ (see Section 2.2 for DOIs).

3.3. Temporal variability of sedimentation in the Northern Gulf of Mexico

At the DWH site, fluxes followed a quasi-seasonal pattern except for $CaCO_3$. $CaCO_3$ fluxes did not show any regularity, but appeared to decrease throughout the sampling period: fluxes were higher and more variable during June 2012–June 2013 (57 ± 56 mg $CaCO_3$ m^{-2} d^{-1}, n = 19) than afterwards (42 ± 25 mg $CaCO_3$ m^{-2} d^{-1}, n = 39). Total mass flux, POC, PON, $bSiO_2$, TEP and lithogenic matter fluxes were highest during March–May 2013, February 2014, January–March 2015 and January–February 2016 (Figure S1d). These dates correspond to the annual winter bloom observed at the DWH site (**Figure 2a**). Based on other evidence (see Section 4.1) we believe that a second, larger export event occurred later in the year, causing the clogging of our traps at the DWH site. Clogs occurred in July 2013, July 2014, April 2015, and February 2016. These clogs caused the loss of all subsequent samples, potentially leading to a significant underestimate of particle flux at the DWH site. No trap clogging was observed earlier, in 2012 (this study) or during 2011 (Yan et al., 2016).

At the Reference site, all fluxes except $CaCO_3$ fluxes peaked in summer (April–May 2012, July 2013, May–July 2014) and were lowest around December (Figure S1). As for the DWH site, $CaCO_3$ fluxes showed no seasonal cycle, but were higher in April–July 2012 (> 40 mg $CaCO_3$ m^{-2} d^{-1}) and consistently lower afterwards.

The Seep site did not show a clear seasonal cycle for any of the fluxes, and fluxes were relatively constant throughout the sampling period. The only exceptions were $CaCO_3$ fluxes in 2012–2013, which were ~4 times higher than during the following years (Figure S1).

In the open ocean, particle flux at depth is generally linked to the production of particles in the surface waters.

Table 2: Averages fluxes and composition at in the Northern Gulf of Mexico in 2012–2016.[a] DOI: https://doi.org/10.1525/elementa.264.t2

Site		Daily Fluxes (mg m^{-2} d^{-1})[b]							Annual Fluxes (g m^{-2} yr^{-1})[c]			
		DW	POC	PON	TEP[d]	$bSiO_2$	$CaCO_3$	Lith	OM[e]	$bSiO_2$	$CaCO_3$	Lith
DWH	avg ± sd	443 ± 347	17 ± 13	2 ± 2	45 ± 44	41 ± 37	47 ± 38	321 ± 289	14 ± 4	18 ± 8	14 ± 2	126 ± 51
	min-max	99 – 2228	5 – 64	0 – 9	2 – 226	9 – 176	0 – 185	52 – 1940				
	%DW		4 ± 1	1 ± 0		9 ± 3	12 ± 8	69 ± 7				
Seep	avg ± sd	255 ± 126	10 ± 5	1 ± 1	26 ± 14	21 ± 13	55 ± 62	160 + 94	8 ± 1	7 ± 2	17 ± 9	54 ± 12
	min-max	27 – 643	1 – 26	0 – 4	3 – 56	4 – 56	0 – 350	0 – 495				
	%DW		4 ± 2	1 ± 0		9 ± 4	21 ± 17	61 ± 15				
Ref.	avg ± sd	103 ± 118	6 ± 5	1 ± 1	13 ± 10	10 ± 11	25 ± 35	58 ± 93	4 ± 1	3 ± 0	6 ± 2	19 ± 5
	min-max	3 – 639	1 – 25	0 – 5	1 – 45	0 – 48	0 – 178	0 – 504				
	%DW		7 ± 4	1 ± 1		9 ± 4	29 ± 31	50 ± 23				

[a] Sediment traps were deployed at ~1400 m depth at three sites (see Table 1 for deployment details).
[b] Average daily fluxes were calculated based on all trap samples.
[c] Average annual fluxes were calculated using running sum (365 days) of interpolated fluxes of individual trap samples.
[d] TEP are measured as Gum Xanthan equivalent, a semi-quantitative measurement. As TEP are part of POC, their contribution to DOC was no calculated.
[e] Organic matter (OM) calculated as (2.2 × POC).

Particle fluxes are often compared to shallower fluxes or PP to characterize the system. For the Seep and Reference sites, we found that PP (as derived from satellite data for an area of ~50 × 50 km² around the traps) and particle flux at depth (**Figure 2**) had no obvious relationship. At the DWH site, POC flux seemed to follow peaks in PP (**Figures 2a**, **d** and **4**). The correlation between POC flux and concurrent PP estimates was significant ($p < 0.01$, n = 58; log-log transformation) but the explained variability in fluxes as a function of PP was low ($R^2 = 0.11$).

3.4. Petrocarbon data

Sinking material at the DWH site (June–September 2012) contained relatively high concentrations of the sum of all measured PAHs (∑PAH) at 0.27 ± 0.04 μg g^{-1} (n = 4), with a high proportion of 4–6-ringed PAHs (**Figure 5**). ∑PAH at the Seep site decreased in concentration throughout the study period, with the highest concentration observed during 10–20 June 2012 (1.8 μg g^{-1}) and lowest in February–March 2013 (< 0.1 μg g^{-1}). This decrease coincided with a decrease of 5–6-ringed and methylated PAHs, and a proportional increase in 3-ringed PAHs (**Figure 5**). Trapped material at the Reference site (April 2012–April 2013) included only low concentrations of ΣPAHs (0.07 ± 0.03 μg g^{-1}, n = 18) which were dominated by low-weight molecular PAHs and no detectable 5–6-ringed PAHs (**Figure 5**). Based on ∑PAH at the Reference site, background levels of ∑PAH concentrations appeared to be < 0.15 μg g^{-1} (maximum concentration observed at the Reference site).

∑PAH fluxes were lowest at the Reference site with a mean of 0.006 ± 0.005 μg m^{-2} d^{-1} (April 2012–April 2013). Fluxes at the DWH site were higher and fairly consistent during the short sampling period (June–September 2012) with a mean of 0.125 ± 0.024 μg m^{-2} d^{-1}. At the Seep site, ∑PAH fluxes had a mean of 0.283 ± 0.041 μg m^{-2} d^{-1} (April 2012–April 2013) and were highly variable, ranging from 0.010 to 0.413 μg m^{-2} d^{-1}. Highest ∑PAH fluxes were observed between April and June 2012 with a maximum of 0.413 μg m^{-2} d^{-1}. The values decreased after June, with average fluxes (over the entire sampling period) of 0.092 ± 0.103 μg m^{-2} d^{-1}. Detailed figures of ΣPAH concentrations, fluxes and compositions of all three sites can be found in the supplementary material (Figures S2–S4).

Non-metric multidimensional scaling (NMDS) analysis of the composition of settled material based on 40 hydrocarbon groups confirmed significant differences between the three sites ($p < 0.01$; **Figure 6**). Whereas hydrocarbon composition remained relatively unchanged over time at the Reference site, there were clear temporal gradients in the hydrocarbon composition of samples within the DWH and Seep sites. For the DWH site, we compared the June–September 2012 samples to those from August 2010–September 2011 (Yan et al., 2016) and found the 2012 samples to be significantly different ($p < 0.02$) from the 2010–2011 samples: petrogenic hydrocarbons, which dominated total hydrocarbons in August–November 2010, decreased in importance from November 2010 to September 2011, and were even less prevalent during our sampling period in 2012 (**Figure 6**).

For the Seep site, we used seven indices to categorize the different time periods observed during 2012–2013 (**Table 4**). Between April and June 2012 (period A), the presence of crude oil was obvious as indicated by the high load of ΣPAH, low Fl/(Fl+Py), and prevalence of long n-alkanes. Within this period, there were strong variations in $C_0/(C_0+C_1)$ and CPI, which indicate combustion, de-methylation, and/or strong influences of biogenic alkanes during 27 April–29 May 2012 (cups 2–4). We distinguished two periods with high ΣPAH load and fluxes (around 16–27 April and 30 May–20 June 2012) as phase A1, and the remainder (27 April–30 May) as phase A2. Between June and August 2012 (period B), the ΣPAH load

Table 3: Coefficient of determination (R^2) between different flux components across all samples. DOI: https://doi.org/10.1525/elementa.264.t3

Flux components[a]	DW (mg m^{-2} d^{-1})	POC (mg m^{-2} d^{-1})	PON (mg m^{-2} d^{-1})	Bsi (mg m^{-2} d^{-1})	Lith (mg m^{-2} d^{-1})	TEP (mg XGeq m^{-2} d^{-1})
POC (mg m^{-2} d)	0.77*** (166)	–	–	–	–	–
PON (mg m^{-2} d)	0.72*** (166)	0.94*** (166)	–	–	–	–
Bsi (mg m^{-2} d)	0.67*** (162)	0.73*** (162)	0.64*** (162)	–	–	–
Lith (mg m^{-2} d)	0.94*** (162)	0.76*** (162)	0.72*** (162)	0.58*** (162)	–	–
TEP (mg XGeq m^{-2} d)	0.56*** (128)	0.55*** (128)	0.42*** (128)	0.55*** (127)	0.52*** (127)	–
$CaCO_3$ (mg m^{-2} d)	0.10*** (166)	n.s.[b] (166)	n.s. (166)	n.s. (162)	n.s. (162)	n.s. (127)

[a] Values show R^2 of the linear regression on untransformed data Values in brackets show number of observations.

*** Three asterisks indicate significance at $p < 0.001$.

[b] *n.s.* indicates significance at $p > 0.05$.

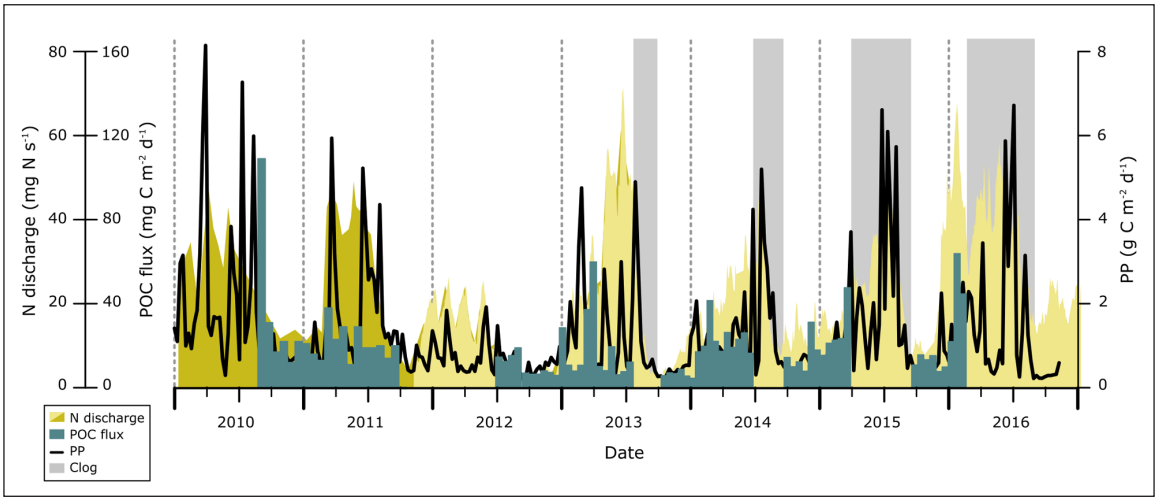

Figure 4: Potential drivers of POC flux at the DWH site. Time series of POC flux at 1540 m depth (green bars) and satellite-derived primary production (PP, black line) at the DWH site. Mississippi River discharge of nitrate + nitrite (N) at Francisville (dark yellow) and Baton Rouge (light yellow), LA. Periods where the trap clogged, likely because of high particle fluxes, are marked in light grey. Dashed grey lines show the first day of each year. DOI: https://doi.org/10.1525/elementa.264.f4

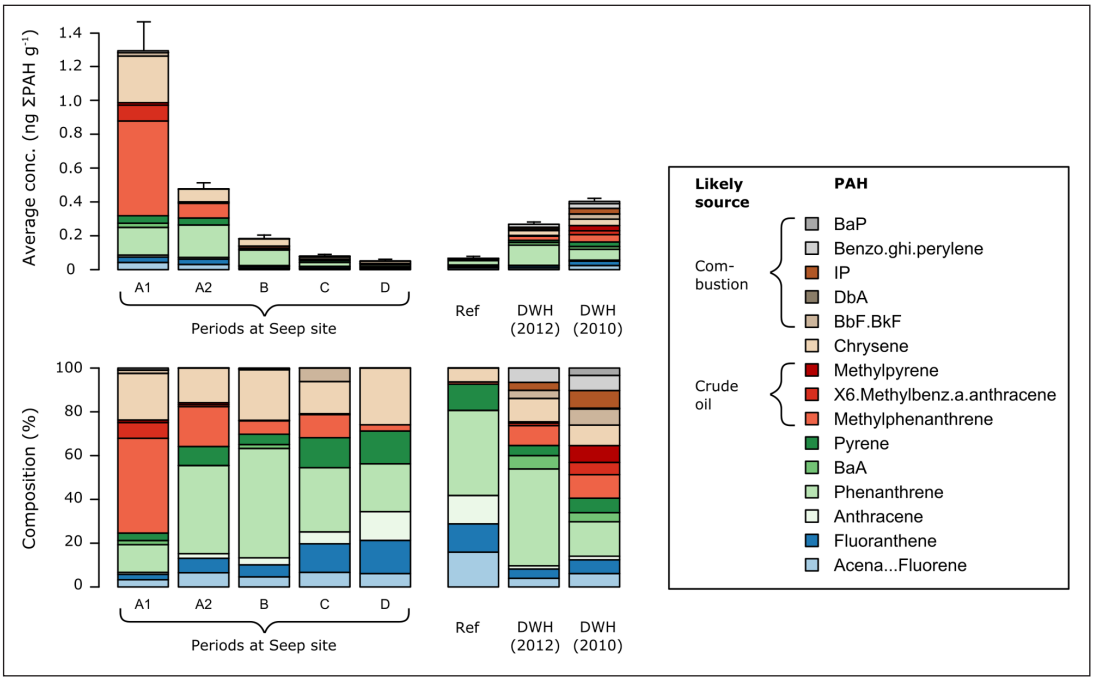

Figure 5: Average ΣPAH concentrations and composition at the Seep site. Average ΣPAH concentrations (top) and composition (bottom) at the Seep site at ~1400 m depth during 2012–2013. PAHs are colored as shown in the inset legend, along with interpretation of potential source. Seep site samples were grouped into five periods, according to seven hydrocarbon indices (see Methods), as containing clear signs of fresh crude oil (A1), weathered crude oil (A2), predominantly combustion products (B), no unusual contamination but an old isotope signal (C), or no unusual contamination (D). Average ΣPAH concentrations and composition at the Reference (Ref) site (April 2012–April 2013) and at the DWH site during June–September 2012 (DWH 2012) and August 2010–September 2011 (DWH 2010) are shown for comparison. Error bars show SD of cups within each period. DOI: https://doi.org/10.1525/elementa.264.f5

decreased to an average of 0.2 ± 0.1 μg g^{-1} (n = 7). The Fl/(Fl+Py) and $C_0/(C_0+C_1)$ values suggest a pyrogenic origin. The CPI was higher than during the preceding period, but during two intervals (20 June–1 July, cup 7; 23 July–14 August, cups 10 and 11) this index suggests the influence of petrogenic sources.

After September 2012 (periods C and D), ΣPAH contamination decreased to levels comparable to the Reference

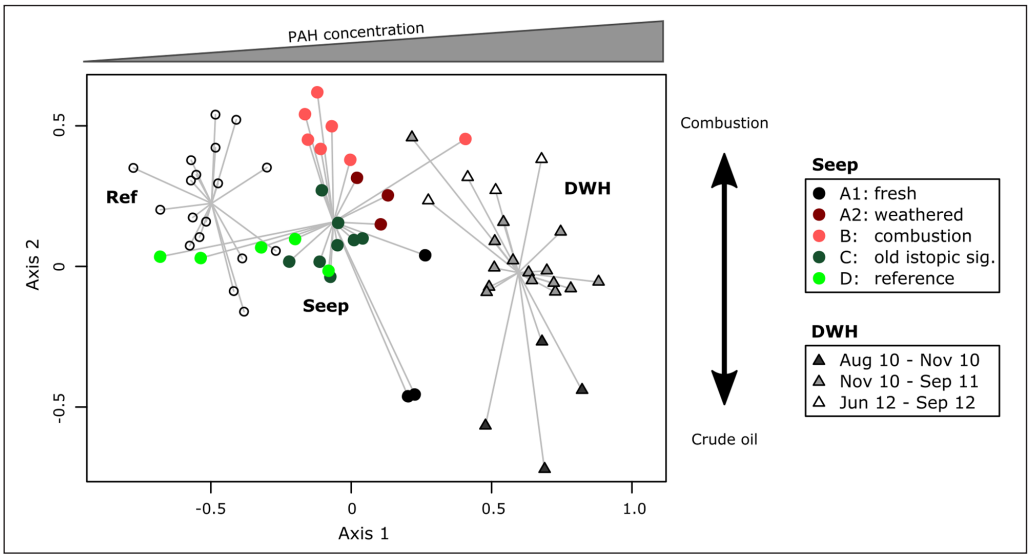

Figure 6: Cluster analysis of hydrocarbons in sediment trap samples collected at the three sites. Data from all sediment trap samples collected at the three sites, at ~1400 m depth in the Northern Gulf of Mexico, during 2010–2011 and 2012–2013 were evaluated using non-metric multidimensional scaling (NMDS). The first axis approximates the gradient in ΣPAH concentrations; the second axis approximates the shift from petrogenic to pyrogenic sources based on methylation and number of aromatic rings. Points closer together have higher similarity. Reference site samples are shown as open circles. Seep site samples are shown as solid circles and categorized, according to seven hydrocarbon indices (see Methods), as containing clear signs of fresh crude oil (A1, black), weathered crude oil (A2, dark red), predominantly combustion products (B, light red), no unusual contamination but an old isotope signal (C, dark green), and no unusual contamination (D, light green). DWH site samples are shown as triangles and colored according to the sampling period (August–November 2010, black; November 2010–September 2011, grey; June–September 2012, white). DOI: https://doi.org/10.1525/elementa.264.f6

site. The low Fl/(Fl+Py) and high $C_0/(C_0+C_1)$ values strongly indicate that all of the PAHs originated from combustion products. The high CPI and low ACL values suggest that the majority of alkanes originated from biological sources. Interestingly, the $\Delta^{14}C$ signal was unusually low between September 2012 and January 2013, and returned to baseline values after January 2013. We distinguished these two periods as C (low $\Delta^{14}C$ signal) and D (high $\Delta^{14}C$ signal), respectively.

These indices correspond well to the ordination of the NMDS analysis (**Figure 6**). According to the NMDS analysis, all periods (A1, A2, B, C and D) were significantly different from each other ($p < 0.03$) except for A2 versus A1 (insufficient data) and A2 versus B ($p = 0.08$). These exceptions reflect a transient period between A1 to B. Lastly, we tested whether period D at the Seep site, which was characterized by the lowest concentrations of ΣPAH, differed significantly from the Reference site, and found no significant difference ($p > 0.05$).

4. Discussion

Deep (>1000 m) sedimentation rates at the three sites in the Northern Gulf of Mexico were markedly different in quality and quantity. Summarizing our analysis below, we conclude that the differences were largely driven by varying degrees of riverine, seepage and oceanic influences, which are determined by the highly variable mesoscale circulation (Liu et al., 2017). The DWH site, which is located ~70 km from the Mississippi River Delta, showed patterns of flux quantity and variability that were apparently stimulated by and also strongly linked to the variability in river discharge. The Seep and Reference sites were more influenced by the circulation pattern of the open Gulf of Mexico and differed in flux magnitude, composition and annual sedimentation rates. These differences were likely controlled by oceanic circulation at the mesoscale (10–300 km scale), and in particular by the position and variability of the Loop Current and Loop Current eddies (Liu et al., 2017). However, local influences, like natural seepage at the Seep site, also had measurable impacts on composition.

4.1. Clogging of the trap at the DWH site

At the DWH site, we observed recurring trap clogging, which could have been caused by several processes, such as large sinking particles or sediment resuspension. Diercks et al. (2017) analysed the current velocities at the DWH trap and observed high currents (23 cm s^{-1}) during the passage of Hurricane Issac. During this time (28 August–2 September 2012), resuspension was observed even at the depth of the DWH trap, yet the trap did not clog. Hence, even during periods of unusually high currents and resuspension, no clogging occurred, likely because resuspended material is mostly composed of mineral matter and tends to promote the formation of small aggregates (Passow and De La Rocha, 2006). We conclude that resuspension was unlikely to have caused the recurring clogging at the DWH site.

Table 4: Classification of particle flux at the Seep site during April 2012–April 2013, with average values from the Reference and DWH sites for comparison. DOI: https://doi.org/10.1525/elementa.264.t4

	Trap information			Polycyclic aromatic hydrocarbons (PAHs)				n-alkanes		POC
Site	Cup	Date[a]	Period[b]	∑PAH contamination ($\mu g\ g^{-1}$)	∑PAH flux ($\mu g\ m^{-2}\ d^{-1}$)	Fl/(Fl+Py)[c]	$C_0/(C_0+C_1)$[d]	CPI[e]	ACL[f]	$\Delta^{14}C$[g]
Seep	1	16/04/2012	A1	1.0	0.32	0.4	0.5	1.4	25.8	−38
	2	27/04/2012	A2	0.5	0.21	0.4	0.8	2.2	26.8	−33
	3	08/05/2012	A2	0.4	0.13	0.4	0.6	1.6	25.9	−28
	4	19/05/2012	A2	0.3	0.08	0.4	0.8	1.9	26.9	−50
	5	30/05/2012	A1	1.1	0.15	0.4	0.2	1.1	25.4	−21
	6	10/06/2012	A1	1.8	0.31	0.5	0.1	1.0	24.9	−25
	7	20/06/2012	B	0.3	0.10	0.5	0.9	1.3	25.8	−9
	8	01/07/2012	B	0.2	0.03	0.5	0.9	1.7	25.7	13
	9	12/07/2012	B	0.1	0.03	0.5	0.9	2.0	25.9	−25
	10	23/07/2012	B	0.2	0.03	0.6	1.0	1.4	24.7	−20
	11	03/08/2012	B	0.1	0.02	0.5	0.9	1.0	25.7	−36
	12	14/08/2012	B	0.2	0.05	0.6	0.8	1.7	25.2	−63
	13	25/08/2012	B	0.2	0.05	0.6	0.9	1.6	23.6	−78
	1	10/09/2012	C	0.1	0.07	0.5	0.8	2.3	24.0	−135
	2	28/09/2012	C	0.1	0.07	0.5	0.8	3.4	23.6	−81
	3	16/10/2012	C	0.1	0.04	0.5	0.6	3.1	23.7	−130
	4	03/11/2012	C	0.0	0.01	0.5	0.8	2.5	23.4	−123
	5	20/11/2012	C	0.1	0.01	0.5	0.6	3.3	21.9	−151
	6	08/12/2012	C	0.1	0.03	0.5	0.7	3.0	24.5	−130
	7	26/12/2012	C	0.1	0.04	0.5	0.7	3.3	24.4	−93
	8	13/01/2013	C	0.0	0.02	0.5	0.9	3.4	25.4	−107
	9	31/01/2013	D	0.1	0.02	0.5	0.7	2.7	25.4	−43
	10	18/02/2013	D	0.0	0.01	0.5	1.0	3.2	18.9	−42
	11	07/03/2013	D	0.0	0.01	0.5	1.0	2.9	18.7	−54
	12	25/03/2013	D	0.1	0.02	0.5	1.0	2.5	23.0	−33
	13	12/04/2013	D	0.1	0.03	0.5	0.8	4.5	22.9	28
Seep[h]	1,5,6	For A1	A1	1.0 ± 0.1	0.26 ± 0.10	0.4 ± 0.0	0.3 ± 0.2	1.2 ± 0.2	25.6 ± 0.3	−30 ± 12
	2–4	For A2	A2	0.8 ± 0.7	0.14 ± 0.07	0.4 ± 0.0	0.6 ± 0.3	1.7 ± 0.5	26.2 ± 0.9	−34 ± 11
	7–13	For B	B	0.2 ± 0.1	0.04 ± 0.03	0.5 ± 0.1	0.9 ± 0.0	1.5 ± 0.3	25.2 ± 0.8	−31 ± 31
	1–8	For C	C	0.1 ± 0.0	0.04 ± 0.02	0.5 ± 0.0	0.7 ± 0.1	3.0 ± 0.4	23.9 ± 1.0	−119 ± 23
	9–13	For D	D	0.1 ± 0.0	0.02 ± 0.01	0.5 ± 0.0	0.9 ± 0.2	3.1 ± 0.8	21.8 ± 2.9	−29 ± 33
DWH[h]	all	all	all	0.3 ± 0.0	0.11 ± 0.02	0.5 ± 0.1	0.8 ± 0.0	2.6 ± 0.5	23.6 ± 1.6	−46 ± 19
Reference[h]	all	all	all	0.1 ± 0.0	0.00 ± 0.01	0.5 ± 0.1	1.0 ± 0.1	4.0 ± 1.6	19.7 ± 1.4	12 ± 29

[a] Date shows collection start date (day/month/year).

[b] Periods were categorized according to hydrocarbon indices and isotopic composition. A1: clear crude oil influence, A2: weathered crude oil, B: strong influence of combustion products, likely with petrogenic sources, C: background level, D: background level with petrogenic age signature.

[c] Ratio of fluoranthene to fluoranthene + pyrene, an index of temperature during formation indicative of source: > 0.5 suggests dominance of pyrogenic PAH sources, < 0.4 suggests dominance of petrogenic PAH sources (see text).

[d] Ratio of parent phenanthrene to phenanthrene plus its monomethyl homologues, an index of de-acylation indicative of process: ≤ 0.5 interpreted as dominance of PAHs from crude oil (see text).

[e] Carbon preference index, an index of biological preference indicative of source.

[f] Average chain length of n-alkanes, indicative of source.

[g] Carbon isotopic composition, indicative of age.

[h] Mean values (± SD), with n values of 3, 3, 7, 8, and 5 for A1, A2, B, C, and D, respectively, at the Seep site, 4 for the DWH site, and 18 for the Reference site.

Instead, the temporal correlation between N discharge, PP and clogging (**Figure 4**) suggests that clogging is related to the surface community. As we do not have samples from the clogged periods, we have no direct information on what organisms may have caused the clog; however, we have indirect evidence strongly supporting our hypothesis that a sedimentation pulse caused the clogs. During the 2015–2016 collection period at the DWH site, we lost all samples after 19 February 2016 (cup 9) because of clogging. During this deployment period, we also deployed a sediment trap at 200 m depth which provided information on what was sinking out of the euphotic zone. The shallow DWH site trap collected highest total mass flux during January 2016 (cups 7 and 8), when the ratio of $bSiO_2$ to POC was unusually high (2.9 ± 0.2 mg mg^{-1}, n = 2, compared to 0.6 ± 0.4, n = 6, in the preceding four months), indicating export linked to diatoms or radiolarians. Microscopic analysis revealed few intact diatom frustules, but hydrolysis of organic matter revealed a great abundance of small $bSiO_2$ fragments, which could be of either diatom or radiolarian origin. Heavy grazing is the most likely explanation for the fragmentation.

Diatom blooms have been linked to the formation of large, sticky aggregates that could cause clogging. Another prime candidate for causing the observed clogging of traps is the filamentous, N-fixing cyanobacterium *Trichodesmium*, which at times is common in the Northern Gulf of Mexico. *Trichodesmium* is known to generate large amounts of TEP during bloom termination (Berman-Frank et al., 2007), potentially causing sedimentation of mucus-rich aggregates (Bar-Zeev et al., 2013). Although *Trichodesmium* would no longer be recognizable in deep traps, their trichomes have been identified in shallower traps (Chen et al., 2003). Clogging could also be caused by large organisms falling into the sediment trap, such as jellyfish, which have increased in abundance in the Gulf of Mexico in recent years and are strongly linked to the Mississippi River discharge (Robinson and Graham, 2013). Lastly, we have observed that aggregates with protozoan (e.g. foraminifera and radiolarians) can be very mucus-rich and sticky at times; however, their role in flux measurements is largely unexplored.

4.2. The role of Mississippi discharge for particle flux (DWH site)

The Mississippi River is a major driver of the nearshore ecosystem in the Northern Gulf of Mexico. It is the largest river in North America, has a catchment area of 3 million km^2 and carries a high sediment load of which ~70% are fine sediments (< 63 μm, silt and clay; Thorne et al., 2008). Concentrations of fine sediments are relatively constant throughout the year, with median concentrations of 150–250 ppm (Thorne et al., 2008). The transport of Mississippi River water within the Gulf of Mexico is highly variable, spatially and temporally, and depends strongly on winds, mesoscale eddies and the loop current system (Schiller et al., 2011; Schiller and Kourafalou, 2014). Based on satellite images, the influence of Mississippi waters can be observed as far away as the Florida Straight (Hu et al., 2005). The freshwater intrusions of the Mississippi can often be detected by an increase in surface chlorophyll concentrations (Hu et al., 2005; Schiller et al., 2011; Schiller and Kourafalou, 2014). Moreover, the influence of Mississippi-derived sediment is clearly visible in the distribution of $CaCO_3$ in seafloor sediments, where a 'tongue' with low-$CaCO_3$ sediments (< 10% $CaCO_3$ of sediment DW) extends from the mouth of the Mississippi River towards the Southeast (Balsam and Beeson, 2003; Ellwood et al., 2006). The DWH site is located directly within this low-$CaCO_3$ region and, consistent with this long term geological signal, its average annual particle flux contained < 10% $CaCO_3$. This low fraction of $CaCO_3$ is a strong indicator that the DWH site is highly impacted by Mississippi discharge.

The influence of Mississippi River discharge is two-fold: (1) the high load of fine sediments and POC may lead to elevated suspended lithogenic and particulate organic material that is available for incorporation into marine snow aggregates, and (2) nutrients transported by the river enhance phytoplankton production. The percentage of lithogenic material in total mass flux at the DWH site varied little (69 ± 7%; n = 56; **Table 2**), suggesting that lithogenic matter was incorporated at a constant fraction. This effect may be because fine sediments (< 63 μm) occur at a relatively constant concentration in the pool of suspended matter originating from the Mississippi outflow (Thorne et al., 2008). As a comparison, fluxes at the Seep and Reference sites, which are farther away from the Mississippi River Delta and are much more influenced by currents (see below), have a lower and more variable lithogenic fraction (60 ± 15% (n = 60) and 50 ± 23% (n = 46) of the total matter flux, respectively). Any POC associated with the lithogenic load could also be transported into the traps, but unlike lithogenic material, POC is reworked and respired during transit. As a result, proportionally less riverine POC will enter the trap than lithogenic matter.

Regarding nutrient transport by the Mississippi River, the links between Mississippi discharge and PP and particle flux at the DWH site appear to be strong. During the period 2010–2016, N discharge by the Mississippi peaked generally once a year in late summer (**Figure 4**). Satellite-derived PP at the DWH site peaked systematically 2–3 weeks after the peak in N discharge (**Figure 4**), strongly suggesting a direct link between the autumn bloom at the DWH site and Mississippi discharge. This link is in line with observations that phytoplankton growth in the Northern Gulf of Mexico is nutrient-limited (Lohrenz et al., 1997; Quigg et al., 2011).

The pattern of POC flux at the DWH site approximately matched PP (**Figure 2a, d**) and Mississippi N discharge (**Figure 4**), though there were some periods of high N discharge and low POC fluxes (most pronounced in spring 2013). The potential link between particle flux and river N discharge was further obscured by the recurrence of trap clogging. Our data suggest that the region around the DWH site experiences a winter bloom typical for the Gulf of Mexico (see Section 4.3) and an annual surface bloom, which is driven by the Mississippi N discharge and can be readily observed by satellites. The surface bloom typically lasts ~3 weeks (based on satellite-derived PP data) and likely leads to large export that clogs the traps. Because of the clogs in our traps, we do not know the magnitude of these bloom export events, but they are potentially higher

than the fluxes we observed with our sediment traps, and could thus be in excess of 100 mg C m^{-2} d^{-1}.

Overall, we propose that particle flux at the DWH site is strongly influenced by the Mississippi River discharge through two discharge processes. (1) The fine lithogenic material from the Mississippi River remains in suspension in the water and is advected with the currents to offshore regions. When marine snow forms, it scavenges and incorporates this material, leading to a transport of non-$CaCO_3$ lithogenic material to the sediment. (2) Discharge of nutrients (in particular nitrate and nitrite) and advection of these nutrients with the currents cause marine organic particle production by fertilizing phytoplankton growth and stimulating the food web. This stimulation of biological activity will promote the formation of marine snow and enhance particle fluxes.

4.3. Seasonal flux pattern at the Seep and Reference sites

The seasonal flux pattern at the Seep and Reference sites (**Figure 2e, f**) had no obvious relationship with PP (**Figure 2b, c**), in stark contrast to the DWH site, where fluxes appeared to be linked to PP. The observed PP climatology at the Seep and Reference sites exhibits the same pattern observed in the open Gulf of Mexico (Muller-Karger et al., 2015): PP is highest in winter and lowest in autumn (**Figure 2b, c**).

High winter PP likely occurs because the light regime in the Gulf of Mexico is sufficient for growth all year round, and the limiting factor for phytoplankton growth is nutrient supply. In winter, when the mixed layer is deepest, nutrient supply is high, allowing increased phytoplankton growth (**Figure 2a–c**). Around summer/autumn, when the mixed layer is shallow, nutrient supply is low resulting in reduced PP (**Figure 2b, c**; Müller-Karger et al., 1991, 2015). A similar pattern has been observed in the South China Sea, where light is not limiting and the combined effect of convective overturn and strong winds extend the mixed layer below the nutricline (Tseng, 2005).

The inverse pattern of PP and flux at the two offshore sites, however, is unusual. Recently, such a delay in sedimentation after a period of high PP has been suggested to be caused by high production of transparent exopolymer particles (TEP) in relation to other particles (Mari et al., 2017). TEP are positively buoyant particles (Azetsu-Scott and Passow, 2004), such that TEP-rich aggregates may not sink (Jennings et al., 2017; Mari et al., 2017). A sinking event of organic matter will be delayed and the organic matter will linger in the surface layer until the remineralization of TEP, thought to be more rapid on average than for POC, permits sinking. Alternatively, seasonal differences in sinking velocity and the associated attenuation of sinking organic matter derived from primary production may cause a mismatch between primary production and deep flux.

Another possibility is that the current regime advected particles from the productive coastal regions to the trap. Analysis of the current and wind data in the Northern Gulf of Mexico suggests a seasonality that directs water from the shelf region towards the Reference site primarily during autumn (Smith and Jacobs, 2005). Particle backtracking models also suggest that particles reaching the trap were sometimes transported laterally over 100 km and that particles arriving at the Reference site trap in September 2012 originated at times from filaments of low salinity waters that wrapped around a Loop Current eddy (Liu et al., 2017). This hypothesis is also supported by the observation that, in regions with strong off-shore currents, transport of suspended POC through lateral advection can be higher than vertical fluxes (Alonso-González et al., 2009). We conclude that the most likely explanation for the unusual relationship between flux and PP at the Seep and Reference sites is lateral advection; e.g., that during summer the currents transport particles from the more productive onshore regions towards the central Gulf of Mexico.

4.4. Source area of sinking aggregates: Lateral advection versus resuspension

While the influence of the Mississippi on flux at > 1000 m depth is relatively constant and predictable at the DWH site, we find that it is more occasional and less predictable at the Seep and Reference sites. The currents in the Northern Gulf of Mexico are highly variable. They are under strong influence of the Loop Current, which is a dominant current feature in the Eastern Gulf of Mexico. The Loop Current regularly sheds an anticyclonic eddy approximately every 6–11 months (Sturges and Leben, 2000), which travels west towards the Mexico shelf, where it dissipates (Vidal et al., 1992). Particle transport in the Northern Gulf of Mexico can thus be variable. Nevertheless, a persistent westward transport of fine sediment particles from the Mississippi has been suggested based on modern seafloor sediments (Balsam and Beeson, 2003), indicating that the Seep and Reference sites might be directly influenced by lithogenic particles from the Mississippi. A model analysis of the two study sites shows that the Seep and Reference sites are positioned in the transit area of the Loop Current eddies, and the source area of particles reaching the traps can be, at times, very large (500–600 km; Liu et al., 2017). Depending on the currents, particles collected at the Seep and Reference sites may have a similar origin and stem from close to the traps (such as the case for particles reaching the trap at the Reference site in January 2013), or may follow very different trajectories and originate from across the Gulf, including regions as far south as 24°N or the shelf area (as the case for particles reaching the Seep site in September 2012; Liu et al., 2017).

Resuspension from below the traps was not an important contribution to flux, as current speeds at the depth of the traps were below 10 cm s^{-1} except during Hurricane Issac (Diercks et al., 2017). Resuspension from shelf slopes, on the other hand, may be a more important process: in 2008, a sediment trap deployed at 700 m depth 25 km to the southwest of the Seep site collected lithogenic matter fluxes of 21 ± 22 mg m^{-2} d^{-1} (n = 28; Richey et al., 2014). These fluxes were lower than those we observed at 1260 m depth during 2012–2016 (160 ± 94 mg m^{-2} d^{-1}; **Table 2**), and indicate the advection of terrestrial material offshore via deep downslope transport (Richey and Tierney, 2016).

The traps at the Seep and Reference sites can thus have a large and diverse source capture area and, depending on the position of the eddies and the Loop Current, may collect particles originating not only from the shelf (where the Mississippi River water is usually present year-round) but also from the central Gulf of Mexico. The central Gulf of Mexico is much less productive than the shelf waters, explaining why the fluxes and the contribution of lithogenic matter to total flux at these sites were overall lower and more variable than those observed at the DWH site (**Table 2**). Nevertheless, riverine inputs are likely still an important source of particles at the Seep and Reference sites (Liu et al., 2017), especially during summer months when waters of riverine origin are more commonly found offshore (Schiller and Kourafalou, 2014).

4.5. Effect of seepage on particle flux

Apart from the quantity and the seasonal flux pattern, varying hydrographic conditions combined with variations in particle sources (including local inputs) strongly affected particle quality. In this section, we evaluate how the quality of sinking hydrocarbons varied between sites and temporally at one site, depending on the source area and local conditions. We focus on fluxes at the Seep site, as this site is located in an active seep region and, depending on the currents, is periodically influenced by the Mississippi discharge. As a comparison we present data on hydrocarbon fluxes observed at the DWH site directly after the spill and two years later, in 2012. Based on the hydrocarbon composition and radiocarbon isotope analysis, four distinct periods at the Seep site could be distinguished, which highlights the complex particle dynamics at this site.

Two time intervals where crude-oil-derived PAHs entered the traps in significant amounts (period A1, **Table 4**) were clearly observed. During these periods, PAH composition was markedly different from the remaining periods and sites (**Figures 5** and **6**) and characterized by a high concentration of methylated PAHs and hopanes which are indicative of fresh crude oil. We suspect that this crude oil was derived from active seeps in the vicinity of the Seep site trap and was scavenged during its ascent by sinking marine snow. As seep activity fluctuates in time (Garcia-Pineda et al., 2010, 2014), seepage is temporally and spatially very heterogeneous. Heterogeneous seepage combined with strongly variable small scale currents (Diercks et al., 2017) likely cause irregular advection of hydrocarbon-enriched waters and explain the intermittent nature of these crude-oil flux periods.

PAHs during the A2 period had similar composition and scores on the Fl/(Fl+Py) index, but fewer of the PAHs were alkylated (**Table 4**) and the $C_0/(C_0+C_1)$ value was higher than during A1. Loss of alkyl groups can be used to identify weathering (Sauer et al., 1998), and $C_0/(C_0+C_1)$ ratios increase during early weathering processes (Yan et al., 2016). These two indicators therefore suggest that particle fluxes during period A2 likely contained crude oil that had undergone a higher degree of weathering than those during A1. Crude oil from natural seeps rises towards the surface, where photo-oxidation, evaporation and biodegradation transform the oil. Natural surface oil slicks are often observed at and around the Seep site (Garcia-Pineda et al., 2010). Incorporation into newly formed marine snow aggregates can then transport this weathered oil back to the seafloor. In addition, the relatively high concentration of phenanthrene (which is preferentially lost during weathering) and the overall composition (**Figures 5** and **6**) suggest that sinking particles during A2 contained a large fraction of PAH from combustion-derived sources similar to those found during period B.

Analysis of the samples during period B indicates that PAHs had pyrogenic sources, though they also carried a weak petrogenic signal (**Table 4**). The most important dispersion route of combustion-derived PAHs is the release into the atmosphere (Abdel-Shafy and Mansour, 2016), from where PAHs are transported with the wind until removed from the atmosphere by either dry (as dust) or wet (with rain) deposition. Combustion-derived PAHs can thus reach the marine environment either directly (aeolian deposition at sea) or indirectly via rivers and groundwater discharge (deposition at land and subsequent run off; Abdel-Shafy and Mansour, 2016).

Similarly, we also observed a high load of combustion-derived PAHs at the DWH site, which makes sense considering the vicinity of the coast, the strong influence from Mississippi discharge in this area, and the particularly high combustion emissions in the Baton Rouge area and generally across the Mississippi catchment area (Caiazzo et al., 2013). An important note is that the ΣPAHs observed at the DWH site in 2012 were likely mostly from combustion and that the concentration of ΣPAHs in the flux material and overall ΣPAHs fluxes were lower (0.27 ± 0.04 μg ΣPAH g^{-1} and 0.11 ± 0.02 mg m^{-2} d^{-1}, n = 4) compared to the fluxes throughout the year after the DWH spill (0.40 ± 0.10 μg ΣPAH g^{-1} and 0.22 ± 0.12 mg m^{-2} d^{-1} (n = 19) during August 2010–October 2011; Yan et al., 2016). However, isotope data also suggest that petrocarbon from the spill was still part of the sinking flux (Chanton et al., 2017).

At the Seep site, an interesting observation was revealed by the isotopic composition of the fluxes. Based on flux composition (both PAHs and biogeochemical composition), fluxes at the Seep site were indistinguishable during periods C and D (**Table 4**). Yet, the isotopic composition shows that the age of carbon in the organic matter during period C was much older. This finding seems contradictory at first, as 'old carbon age' is associated with crude oil. However, isotopes measure fossil carbon regardless of its current chemical state. When petrocarbon is incorporated into the marine food web (Chanton et al., 2012, 2015), the chemical composition of the organic carbon changes but the isotopic signature is retained. In other words, the carbon might not look like the original source (e.g., crude oil) anymore. We thus believe that during this period, released crude oil was biodegraded and taken up by the planktonic food web in sufficient amounts to alter the bulk isotopic composition. Subsequent organic matter production and sedimentation thus carried the age signal of the seepage.

Overall, our time series at Seep site illustrates comprehensively the different pathways that naturally released crude oil can take. Released crude oil may never reach the sea surface, instead being scavenged by sinking particles and returned to the benthos, or it may reach the surface where it undergoes weathering before being scavenged into marine snow and sinking, retaining most of its original signal (periods A1 and A2). Or it may enter the food web and sink in a completely different form, e.g., as detritus (period C). Small seepage, strong weathering and mixing with pyrogenic sources may obscure the presence of crude oil from seeps either by diluting or altering the composition (period B).

The high variability of hydrocarbon composition at the different sites and over time (particularly at the Seep site) clearly highlights the dynamic nature of the Northern Gulf of Mexico system. The hydrocarbon composition illustrates that the quality of particle flux is strongly influenced by transport processes like currents and winds, as well as by particle sources like natural seeps, primary production, and riverine material. Our data show that the quality of sinking particles can vary dramatically over short spatial and temporal scales, even if the main components of flux (POC, PON, $bSiO_2$ and lithogenic matter) are relatively constant.

4.6. Was the flux event in September 2010, after DWH, unusual?

One of the problems in the aftermath of the DWH oil spill was the lack of a baseline for the Gulf of Mexico ecosystem. Sediment core analysis shows that large amounts of oil were deposited on the seafloor (Larson et al., 2013; Valentine et al., 2014; Brooks et al., 2015; Chanton et al., 2015). High fluxes of PAHs associated with crude oil were also found in sediment trap samples collected during August–November 2010 just after the well was sealed (15 July 2010; Yan et al., 2016). POC flux of the first of these samples was also 2–3 times higher than fluxes observed the 2 years afterwards, which leads to the suggestion that oil and black carbon promoted aggregation and more effective sedimentation. Whether the crude oil that was transported to the seafloor in September 2010 was carried by unusually high export fluxes or whether baseline export fluxes effectively collected large amounts of oil during aggregation and sinking through the water column is not clear. Unfortunately, no sediment traps in the near vicinity of DWH were deployed during the oil spill, so no direct measurement of total mass flux during the spill is available. However, our long-term time series of trap deployments at the DWH site gives us a good idea of the interannual variability and the drivers of particle flux in the Northern Gulf of Mexico.

Our data suggest that annual peak fluxes are often in excess of 100 mg C m^{-2} d^{-1}. This excess, in turn, means that the magnitude of the high flux event in September 2010 (109 mg C m^{-2} d^{-1}; Yan et al., 2016) was not unusual, but potentially typical for this site after N discharge. Peak N fluxes vary from year to year, but 2010 was similar to the years 2011, 2014 and 2015. In 2012, a drought caused unusually low N discharge (**Figure 4**; Van Metre et al., 2016), which explains why we did not observe high fluxes in 2012, and why Yan et al. (2016) deduced that the September 2010 flux was unusually high. This example illustrates how critical long-term monitoring is to fully understand export mechanisms and flux drivers.

Yet, the flux composition at the DWH site was different in September 2010 compared to the rest of our time series, suggesting that the export mechanism may have been different to other periods. The high accumulation rates of settled material on the seafloor also suggest that the annual sedimentation rate was elevated in 2010 compared to other years. Fluxes during September 2010 were very high in terms of $bSiO_2$ (400 mg $bSiO_2$ m^{-2} d^{-1} and 25% of total matter flux; Yan et al., 2016) and contained much less lithogenic matter (46% instead of the typical 70 ± 8%). These findings are in line with the observation that the high flux in September 2010 contained a high number of diatoms. There are two obvious explanations for the atypical flux composition: (1) the September 2010 flux contained additional C from sources atypical for the DWH site and related to the oil spill, or (2) the September 2010 flux was the tail end of several large sedimentation events which had collected and exported most suspended lithogenic matter from the water column.

One possibility is that additional POC was exported after the DWH oil spill that was atypical for the DWH site. The diatom aggregates in September 2010 could have collected the large aggregates that were observed in the water column (Daly et al., 2016) and formed as a response to the oil and dispersant (Passow et al., 2012; Joye et al., 2014). This trap contained a high proportion of oil-spill related carbon: e.g., black carbon made up 8% of the POC flux (Yan et al., 2016).

More likely, however, is our second hypothesis. During the DWH oil spill, several large flux events were observed that carried a significant fraction of the spilled oil and *in situ* burning residues to depth. The first of these events was likely caused by dead planktonic organisms (Passow et al., 2012) that were blooming during this time (**Figure 4**). Later, marine snow formation was likely caused by oil-degrading bacteria (Passow et al., 2012; Joye et al., 2014; Valentine et al., 2014; Chanton et al., 2015), eventually followed by the phytoplankton-driven export events such as the one observed in September 2010 (Yan et al., 2016). During this series of export events, marine snow formation may have incorporated most of the suspended lithogenic matter. If the resupply rate of suspended sediment matter by lateral advection and aeolian input was slower than incorporation into marine snow and subsequent export, aggregates formed in September 2010 would have incorporated much less lithogenic matter than usual. As a result, the POC-to-lithogenic matter ratio would be higher than during the other export events, which was indeed the case (10% in September 2010 compared to 5 ± 1% in the following 12 months). Modeling work based on coagulation theory, in which aggregation and sinking of a diatom bloom are simulated, suggests that the September 2010 trap collected the tail end of a large export event that

happened shortly before the sampling period (Francis & Passow, pers. communication). Overall, we conclude that the magnitude of the total flux in September 2010 was not unusual, but that the composition differed with a clear petrocarbon signal.

5. Summary

Sedimentation dynamics in the Northern Gulf of Mexico are complex. Aggregation and export are enhanced in regions influenced by the Mississippi River, as its nitrogen discharge allows high phytoplankton growth in the otherwise nutrient-limited Northern Gulf of Mexico. We observed such tight coupling at the DWH site, where seasonality and quantity of flux reflected Mississippi discharge and subsequent primary production. A surface bloom, which was observed annually following the peak discharge in nitrogen, likely caused export events.

At our two offshore sites, fluxes did not reflect primary production and did not show a clear seasonality. The particle source regions for these sites were large and diverse, owing to strong currents and mesoscale circulation (Loop Current and numerous eddies). At these sites, low salinity, nitrogen-rich riverine waters and marine snow aggregates are at times carried for hundreds of kilometers before reaching the bathypelagic and/or seafloor (Liu et al., 2017). Sites in less productive regions, such as our two offshore sites, may thus be episodically exposed to high organic matter fluxes that are similar in magnitude and composition to fluxes at more coastal regions.

At all sites, total mass flux at ~1400 m depth predominantly consisted of lithogenic material (50–70%), which likely originated from the Mississippi plume. Organic matter, $CaCO_3$ and $bSiO_2$ made up the remainder with approximately equal contributions. The relative composition of inorganic material in the three traps reflects the respective composition in sediments below the traps (Balsam and Beeson, 2003).

Depending on the location and the state of the currents, marine snow also carried varying amounts and compositions of PAHs to depth. Our data show that the DWH site carried a relatively high load of petrogenic PAHs (compared to our Reference site), likely owing to its close vicinity to the shore and the strong influence by the Mississippi River plume. Comparison of our time series with the sediment trap samples collected during the year following the DWH oil spill (August 2010–October 2011; Yan et al., 2016) suggests that the particle fluxes had not recovered to baseline levels by October 2011 (Chanton et al., 2017).

In the vicinity of natural seeps, PAH fluxes tended to be higher than at our Reference site but lower and of different origin than at the DWH site. We also observed indications of three different pathways for "natural" oiled-snow sedimentation. First, fluxes at times contained a strong oil signal, which was likely caused by natural seepage that was incorporated into sinking aggregates; however, such events were episodic, highlighting the heterogeneity of seepage and currents. Second, combustion products dominated at other times, possibly introduced by advection from coastal areas. Last, PAH fluxes were similar to the Reference site, but isotopic composition suggested that the sinking carbon originated from oil seepage that had entered the food web and was converted to organic matter, hence losing the chemical oil signature but retaining the isotopic composition.

Data Accessibility Statement

Data are publicly available through the Gulf of Mexico Research Initiative Information & Data Cooperative (GRIIDC) at https://data.gulfresearchinitiative.org.

Supplemental Files

The supplemental files for this article can be found as follows:

- **Table S1.** List of analyzed hydrocarbons. DOI: https://doi.org/10.1525/elementa.264.s1
- **Figure S1.** Particle flux rates in the Northern Gulf of Mexico at the Reference, Seep and DWH sites. https://doi.org/10.1525/elementa.264.s1
- **Figure S2.** Polycyclic aromatic hydrocarbons at the DWH site during August 2010–September 2012 and June–August 2012 (last four bars). https://doi.org/10.1525/elementa.264.s1
- **Figure S3.** Polycyclic aromatic hydrocarbons at the Seep site during April 2012–April 2013. https://doi.org/10.1525/elementa.264.s1
- **Figure S4.** Polycyclic aromatic hydrocarbons at the Reference site during April 2012–April 2013. https://doi.org/10.1525/elementa.264.s1

Acknowledgements

We thank the captain and crew of the RV *Oceanus* for help with the deployment of the sediment traps. We also thank Prof Jody Deming for valuable editing.

Funding information

This research was made possible by a grant from The Gulf of Mexico Research Initiative to support the "Ecosystem Impacts of Oil and Gas in the Gulf" (ECOGIG) research consortium. This is ECOGIG contribution number 486.

Competing interests

The authors have no competing interests to declare.

Author contributions

- Contributed to conception and design: UP, VA
- Contributed to acquisition of data: UP, VA, AD, JS, JC, BY, MP
- Contributed to analysis and interpretation of data: SG, UP, BY
- Drafted and/or revised the article: SG, UP
- Approved the submitted version for publication: all

References

Abdel-Shafy, HI and **Mansour, MSM** 2016 A review on polycyclic aromatic hydrocarbons: Source, environmental impact, effect on human health

and remediation. *Egypt J Pet* **25**(1): 107–123. DOI: https://doi.org/10.1016/j.ejpe.2015.03.011

Alonso-González, IJ, Arístegui, J, Lee, C, Sanchez-Vidal, A and **Calafat, A,** et al. 2010 Role of slowly settling particles in the ocean carbon cycle. *Geophys Res Lett* **37**(13): n/a-n/a. DOI: https://doi.org/10.1029/2010GL043827

Alonso-González, IJ, Arístegui, J, Vilas, JC, Hernández-Guerra, A 2009 Lateral POC transport and consumption in surface and deep waters of the Canary Current region: A box model study. *Global Biogeochem Cycles* **23**(2): 1–12. DOI: https://doi.org/10.1029/2008GB003185

Amante, C and **Eakin, BW** 2009 ETOPO1 1 Arc-Minute Global Relief Model: Procedures, Data Sources and Analysis. NOAA Technical Memorandum NESDIS NGDC-24.

Anderson, MJ 2001 A new method for non-parametric multivariate analysis of variance. *Austral Ecol* **26**(1): 32–46. Blackwell Science Pty. DOI: https://doi.org/10.1111/j.1442-9993.2001.01070.pp.x

Anderson, MJ 2006 Distance-Based Tests for Homogeneity of Multivariate Dispersions. *Biometrics* **62**(1): 245–253. Blackwell Publishing. DOI: https://doi.org/10.1111/j.1541-0420.2005.00440.x

Azetsu-Scott, K and **Passow, U** 2004 Ascending marine particles: Significance of transparent exopolymer particles (TEP) in the upper ocean. *Limnol Oceanogr* **49**(3): 741–748. DOI: https://doi.org/10.4319/lo.2004.49.3.0741

Baker, A de C, Boden, BP and **Brinton, E** 1990 *A Practical Guide to the Euphausiids of the World*. London: British Museum (Natural History).

Baker, JE, Eisenreich, SJ and **Eadie, BJ** 1991 Sediment trap fluxes and benthic recycling of organic carbon, polycyclic aromatic hydrocarbons, and polychlorobiphenyl congeners in Lake Superior. *Environ Sci Technol* **25**(3): 500–509. American Chemical Society. DOI: https://doi.org/10.1021/es00015a019

Balsam, WL and **Beeson, JP** 2003 Sea-floor sediment distribution in the Gulf of Mexico. *Deep Sea Res Part I Oceanogr Res Pap* **50**(12): 1421–1444. DOI: https://doi.org/10.1016/j.dsr.2003.06.001

Bar-Zeev, E, Avishay, I, Bidle, KD and **Berman-Frank, I** 2013 Programmed cell death in the marine cyanobacterium *Trichodesmium* mediates carbon and nitrogen export. *ISME J* **7**(12): 2340–2348. DOI: https://doi.org/10.1038/ismej.2013.121

Behrenfeld, MJ and **Falkowski, PG** 1997 Photosynthetic rates derived from satellite-based chlorophyll concentration. *Limnol Oceanogr* **42**(1): 1–20. DOI: https://doi.org/10.4319/lo.1997.42.1.0001

Berman-Frank, I, Rosenberg, G, Levitan, O, Haramaty, L and **Mari, X** 2007 Coupling between autocatalytic cell death and transparent exopolymeric particle production in the marine cyanobacterium *Trichodesmium*. *Environ Microbiol* **9**(6): 1415–1422. DOI: https://doi.org/10.1111/j.1462-2920.2007.01257.x

Blumer, M 1976 Polycyclic aromatic compounds in nature. *Sci Am* **234**(3): 35–45. Available at: http://www.ncbi.nlm.nih.gov/pubmed/1251182. Accessed 2017 Mar 3. DOI: https://doi.org/10.1038/scientificamerican0376-34

Boyd, PW and **Trull, TW** 2007 Understanding the export of biogenic particles in oceanic waters: Is there consensus? *Prog Oceanogr* **72**(4): 276–312. DOI: https://doi.org/10.1016/j.pocean.2006.10.007

Broman, D, Colmsjö, A, Ganning, B, Näf, C, Zebühr, Y, et al. 1987 "Fingerprinting" petroleum hydrocarbons in bottom sediment, plankton, and sediment trap collected seston. *Mar Pollut Bull* **18**(7): 380–388. DOI: https://doi.org/10.1016/0025-326X(87)90317-1

Brooks, GR, Larson, RA, Schwing, PT, Romero, I, Moore, C, et al. 2015 Sedimentation Pulse in the NE Gulf of Mexico following the 2010 DWH Blowout. Chin W-C, (ed.) *PLoS One* **10**(7): e0132341. DOI: https://doi.org/10.1371/journal.pone.0132341

Budzinski, H, Jones, I, Bellocq, J, Piérard, C and **Garrigues, P** 1997 Evaluation of sediment contamination by polycyclic aromatic hydrocarbons in the Gironde estuary. *Mar Chem* **58**(1–2): 85–97. DOI: https://doi.org/10.1016/S0304-4203(97)00028-5

Buesseler, KO, Trull, TW, Steinberg, DK, Silver, MW, Siegel, DA, et al. 2008 VERTIGO (VERtical Transport In the Global Ocean): A study of particle sources and flux attenuation in the North Pacific. *Deep Sea Res Part II Top Stud Oceanogr* **55**(14–15): 1522–1539. DOI: https://doi.org/10.1016/j.dsr2.2008.04.024

Caiazzo, F, Ashok, A, Waitz, IA, Yim, SHL and **Barrett, SRH** 2013 Air pollution and early deaths in the United States. Part I: Quantifying the impact of major sectors in 2005. *Atmos Environ* **79**: 198–208. DOI: https://doi.org/10.1016/j.atmosenv.2013.05.081

Chanton, J, Zhao, T, Rosenheim, BE, Joye, S, Bosman, S, et al. 2015 Using natural abundance radiocarbon to trace the flux of petrocarbon to the seafloor following the Deepwater Horizon oil spill. *Environ Sci Technol* **49**(2): 847–854. DOI: https://doi.org/10.1021/es5046524

Chanton, JP, Cherrier, J, Wilson, RM, Sarkodee-Adoo, J, Bosman, S, et al. 2012 Radiocarbon evidence that carbon from the Deepwater Horizon spill entered the planktonic food web of the Gulf of Mexico. *Environ Res Lett* **7**(4): 45303. DOI: https://doi.org/10.1088/1748-9326/7/4/045303

Chanton, JP, Giering, S, Bosman, S, Rogers, K, Sweet, J, Asper, V, Diercicks, AR and **Passow, U** 2017 Isotopic composition of sinking particles: Oil effects, recovery and baselines in the Gulf of Mexico, 2010-2016. *Elem Sci Anth* (under review).

Chen, Y, Chen, H and **Lin, Y** 2003 Distribution and downward flux of *Trichodesmium* in the South China Sea as influenced by the transport from the Kuroshio Curren. *Mar Ecol Prog Ser* **259**: 47–57. DOI: https://doi.org/10.3354/meps259047

Daly, KL, Passow, U, Chanton, J and **Hollander, D** 2016 Assessing the impacts of oil-associated marine snow formation and sedimentation during and after the Deepwater Horizon oil spill. *Anthropocene* **13**: 18–33. DOI: https://doi.org/10.1016/j.ancene.2016.01.006

Davies, AJ, Duineveld, GCA, Van Weering, TCE, Mienis, F, Quattrini, AM, et al. 2010 Short-term environmental variability in cold-water coral habitat at Viosca Knoll, Gulf of Mexico. *Deep Sea Res Part I Oceanogr Res Pap* **57**(2): 199–212. DOI: https://doi.org/10.1016/j.dsr.2009.10.012

De La Rocha, CL and **Passow, U** 2007 Factors influencing the sinking of POC and the efficiency of the biological carbon pump. *Deep Sea Res Part II Top Stud Oceanogr* **54**(5–7): 639–658. DOI: https://doi.org/10.1016/j.dsr2.2007.01.004

DeMaster, DJ 1981 The supply and accumulation of silica in the marine environment. *Geochim Cosmochim Acta* **45**(10): 1715–1732. DOI: https://doi.org/10.1016/0016-7037(81)90006-5

Diercks, AR, Dike, C, Asper, VL, DiMarco, SF, Chanton, J and **Passow, U** Resuspension scales in the Northern Gulf of Mexico. *Elem Sci Anth* (under review)

Doughty, CL, Quattrini, AM and **Cordes, EE** 2014 Insights into the population dynamics of the deep-sea coral genus Paramuricea in the Gulf of Mexico. *Deep Sea Res Part II Top Stud Oceanogr* **99**: 71–82. DOI: https://doi.org/10.1016/j.dsr2.2013.05.023

D'souza, NA, Subramaniam, A, Juhl, AR, Hafez, M, Chekalyuk, A, et al. 2016 Elevated surface chlorophyll associated with natural oil seeps in the Gulf of Mexico. *Nat Geosci* **9**(3): 215–218. Nature Research. DOI: https://doi.org/10.1038/ngeo2631

Ellwood, BB, Balsam, WL and **Roberts, HH** 2006 Gulf of Mexico sediment sources and sediment transport trends from magnetic susceptibility measurements of surface samples. *Mar Geol* **230**(3–4): 237–248. DOI: https://doi.org/10.1016/j.margeo.2006.05.008

Fisher, CR, Demopoulos, AWJ, Cordes, EE, Baums, IB, White, HK, et al 2014 Coral Communities as Indicators of Ecosystem-Level Impacts of the Deepwater Horizon Spill. *Bioscience* **64**(9): 796–807. Oxford University Press. DOI: https://doi.org/10.1093/biosci/biu129

Fisher, CR, Hsing, P-Y, Kaiser, CL, Yoerger, DR, Roberts, HH, et al. 2014. Footprint of Deepwater Horizon blowout impact to deep-water coral communities. *Proc Natl Acad Sci U S A* **111**(32): 11744–9. National Academy of Sciences. DOI: https://doi.org/10.1073/pnas.1403492111

Garcia-Pineda, O, MacDonald, I and **Shedd, W** 2014 Analysis of oil-volume fluxes of hydrocarbon-seep formations on the Green Canyon and Mississippi Canyon: A study with 3D-seismic attributes in combination with satellite and acoustic data. *SPE Reserv Eval Eng* **17**(4): 430–435. DOI: https://doi.org/10.2118/169816-PA

Garcia-Pineda, O, MacDonald, I, Zimmer, B, Shedd, B and **Roberts, H** 2010 Remote-sensing evaluation of geophysical anomaly sites in the outer continental slope, northern Gulf of Mexico. *Deep Sea Res Part II Top Stud Oceanogr* **57**(21–23): 1859–1869. DOI: https://doi.org/10.1016/j.dsr2.2010.05.005

Gardner, W 1980 Sediment trap dynamics and calibration: a laboratory evaluation. *J Mar Res*, in press. Available at: https://www.researchgate.net/profile/Wilford_Gardner/publication/261510474_Sediment_trap_dynamics_and_calibration_a_laboratory_evaluation/links/0deec5346eb9a261aa000000/Sediment-trap-dynamics-and-calibration-a-laboratory-evaluation.pdf. Accessed 2017 Sep 7.

Hites, RA and **Eisenreich, SJ,** (eds.) 1987 *Sources and Fates of Aquatic Pollutants*. Washington, DC: American Chemical Society. (Advances in Chemistry; Vol. 216). DOI: https://doi.org/10.1021/ba-1987-0216

Honjo, S 1980 Material fluxes and modes of sedimentation in the mesopelagic and bathypelagic zones. *J Mar Res* **38**(1): 53–97.

Honjo, S, Manganini, SJ, Krishfield, R and **Francois, R** 2008 Particulate organic carbon fluxes to the ocean interior and factors controlling the biological pump: A synthesis of global sediment trap programs since 1983. *Prog Oceanogr* **76**(3): 217–285. DOI: https://doi.org/10.1016/j.pocean.2007.11.003

Hu, C, Nelson, JR, Johns, E, Chen, Z, Weisberg, RH and **Müller-Karger, FE** 2005 Mississippi River water in the Florida Straits and in the Gulf Stream off Georgia in summer 2004. *Geophys Res Lett* **32**(14): n/a-n/a. DOI: https://doi.org/10.1029/2005GL022942

Jennings, MK, Passow, U, Wozniak, AS and **Hansell, DA** 2017 Distribution of transparent exopolymer particles (TEP) across an organic carbon gradient in the western North Atlantic Ocean. *Mar Chem* **190**: 1–12. DOI: https://doi.org/10.1016/j.marchem.2017.01.002

Joye, SB, Teske, AP and **Kostka, JE** 2014 Microbial dynamics following the Macondo Oil Well Blowout across Gulf of Mexico environments. *Bioscience* **64**(9): 766–777. DOI: https://doi.org/10.1093/biosci/biu121

Klaas, C and **Archer, DE** 2002 Association of sinking organic matter with various types of mineral ballast in the deep sea: Implications for the rain ratio. *Global Biogeochem Cycles* **16**(4): 63-1–63-14. DOI: https://doi.org/10.1029/2001GB001765

Larson, R, Gregg, B, Patrick, S, David, H, Isabel, R, et al. 2013 Shift in sedimentation patterns and increased mass accumulation rates following the BP Blowout event: NE Gulf of Mexico. 2013 Gulf of Mexico Oil Spill & Ecosystem Conference New Orleans.

Lee, RF and **Page, DS** 1997 Petroleum hydrocarbons and their effects in subtidal regions after major oil spills. *Mar Pollut Bull* **34**(11): 928–940. DOI: https://doi.org/10.1016/S0025-326X(97)00078-7

Lipiatou, E, Marty, J-C and **Saliot, A** 1993 Sediment trap fluxes of polycyclic aromatic hydrocarbons in the Mediterranean Sea. *Mar Chem* **44**(1): 43–54. DOI: https://doi.org/10.1016/0304-4203(93)90005-9

Liu, G, Bracco, A and **Passow, U** 2017 Mesoscale and submesoscale circulation influences sinking particles in the northern Gulf of Mexico. *Elem Sci Anth* (under review).

Lohrenz, SE, Lang, GA and **Chen, X** 1997 Variations in primary production of northern Gulf of Mexico continental shelf waters linked to nutrient inputs from the Mississippi River. **155**: 45–54.

Macdonald, IR, Guinasso, NL, Ackleson, SG, Amos, JF, Duckworth, R, et al. 1993 Natural oil slicks in the Gulf of Mexico visible from space. *J Geophys Res* **98**(C9): 16351. DOI: https://doi.org/10.1029/93JC01289

MacDonald, IR, Leifer, I, Sassen, R, Stine, P, Mitchell, R, et al. 2002 Transfer of hydrocarbons from natural seeps to the water column and atmosphere. *Geofluids* **2**(2): 95–107. Blackwell Science, Ltd. DOI: https://doi.org/10.1046/j.1468-8123.2002.00023.x

Mari, X, Passow, U, Migon, C, Burd, AB and **Legendre, L** 2017 Transparent exopolymer particles: Effects on carbon cycling in the ocean. *Prog Oceanogr* **151**: 13–37. DOI: https://doi.org/10.1016/j.pocean.2016.11.002

Martin, JH, Knauer, GA, Karl, DM and **Broenkow, WW** 1987 VERTEX: carbon cycling in the northeast Pacific. *Deep Sea Res I* **34**(2): 267–285. DOI: https://doi.org/10.1016/0198-0149(87)90086-0

McDonnell, AMP and **Buesseler, KO** 2010 Variability in the average sinking velocity of marine particles. *Limnol Oceanogr* **55**(5): 2085–2096. DOI: https://doi.org/10.4319/lo.2010.55.5.2085

McNichol, AP and **Aluwihare, LI** 2007 The power of radiocarbon in biogeochemical studies of the marine carbon cycle: Insights from studies of dissolved and particulate organic carbon (DOC and POC). *Chem Rev* **107**(2): 443–466. DOI: https://doi.org/10.1021/cr050374g

Mienis, F, Duineveld, GCA, Davies, AJ, Ross, SW, Seim, H, et al. 2012 The influence of near-bed hydrodynamic conditions on cold-water corals in the Viosca Knoll area, Gulf of Mexico. *Deep Sea Res Part I Oceanogr Res Pap* **60**: 32–45. DOI: https://doi.org/10.1016/j.dsr.2011.10.007

Mortlock, RA and **Froelich, PN** 1989 A simple method for the rapid determination of biogenic opal in pelagic marine sediments. *Deep Sea Res Part A Oceanogr Res Pap* **36**(9): 1415–1426. DOI: https://doi.org/10.1016/0198-0149(89)90092-7

Muller-Karger, FE, Smith, JP, Werner, S, Chen, R, Roffer, M, et al. 2015 Natural variability of surface oceanographic conditions in the offshore Gulf of Mexico. *Prog Oceanogr* **134**: 54–76. DOI: https://doi.org/10.1016/j.pocean.2014.12.007

Müller-Karger, FE, Walsh, JJ, Evans, RH and **Meyers, MB** 1991 On the seasonal phytoplankton concentration and sea surface temperature cycles of the Gulf of Mexico as determined by satellites. *J Geophys Res* **96**(C7): 12645. DOI: https://doi.org/10.1029/91JC00787

Oksanen, J, Blanchet, FG, Friendly, M, Kindt, R, Legendre, P, et al. 2016 vegan: Community Ecology Package. Available at: http://cran.r-project.org/package=vegan.

Paasivirta, J, Kääriäinen, H, Lahtiperä, M, Pellinen, J and **Sinkkonen, S** 1982 Oil residues in Baltic sediment, mussel and fish. II. Study of the Finnish Archipelago 1979–1981. *Chemosphere* **11**(8): 811–821. DOI: https://doi.org/10.1016/0045-6535(82)90110-2

Passow, U and **Alldredge, AL** 1995 A dye-binding assay for the spectrophotometric measurement of transparent exopolymer particles (TEP). *Limnol Oceanogr* **40**(7): 1326–1335. DOI: https://doi.org/10.4319/lo.1995.40.7.1326

Passow, U and **De La Rocha, CL** 2006 Accumulation of mineral ballast on organic aggregates. *Global Biogeochem Cycles* **20**(1): n/a-n/a. DOI: https://doi.org/10.1029/2005GB002579

Passow, U, Shipe, R, Murray, A, Pak, D, Brzezinski, M, et al. 2001 The origin of transparent exopolymer particles (TEP) and their role in the sedimentation of particulate matter. *Cont Shelf Res* **21**(4): 327–346. DOI: https://doi.org/10.1016/S0278-4343(00)00101-1

Passow, U and **Ziervogel, K** 2016 Marine snow sedimented oil released during the Deepwater Horizon spill. *Oceanography* **29**(3): 118–125. DOI: https://doi.org/10.5670/oceanog.2016.76

Passow, U, Ziervogel, K, Asper, V and **Diercks, A** 2012 Marine snow formation in the aftermath of the Deepwater Horizon oil spill in the Gulf of Mexico. *Environ Res Lett* **7**(3): 35301. IOP Publishing. DOI: https://doi.org/10.1088/1748-9326/7/3/035301

Poynter, J and **Eglinton, G** 1990 Molecular Composition of Three Sediments from Hole 717C: The Bengal Fan. In: *Proceedings of the Ocean Drilling Program, 116 Scientific Results*. Ocean Drilling Program. DOI: https://doi.org/10.2973/odp.proc.sr.116.151.1990

Prouty, NG, Campbell, PL, Mienis, F, Duineveld, G, Demopoulos, AWJ, et al. 2016 Impact of Deepwater Horizon spill on food supply to deep-sea benthos communities. *Estuar Coast Shelf Sci* **169**: 248–264. DOI: https://doi.org/10.1016/j.ecss.2015.11.008

Quigg, A, Sylvan, JB, Gustafson, AB, Fisher, TR, Oliver, RL, et al. 2011 Going West: Nutrient limitation of primary production in the Northern Gulf of Mexico and the importance of the Atchafalaya River. *Aquat Geochemistry* **17**(4–5): 519–544. DOI: https://doi.org/10.1007/s10498-011-9134-3

R Core Team 2015 R: A Language and Environment for Statistical Computing. Vienna, Austria. Available at: http://www.r-project.org/.

Richey, JN, Reynolds, CE, Tappa, E and **Thunell, R** 2014 Weekly resolution particulate flux from a sediment trap in the northern Gulf of Mexico, 2008–2012. Open-File Report. DOI: https://doi.org/10.3133/ofr20141035

Richey, JN and **Tierney, JE** 2016 GDGT and alkenone flux in the northern Gulf of Mexico: Implications for the TEX 86 and U K' 37 paleothermometers. *Paleoceanography* **31**(12): 1547–1561. DOI: https://doi.org/10.1002/2016PA003032

Roberts, HH, Feng, D and **Joye, SB** 2010 Cold-seep carbonates of the middle and lower continental slope, northern Gulf of Mexico. *Deep Sea Res Part II Top Stud Oceanogr* **57**(21–23): 2040–2054. DOI: https://doi.org/10.1016/j.dsr2.2010.09.003

Robinson, KL and **Graham, WM** 2013 Long-term change in the abundances of northern Gulf of Mexico scyphomedusae *Chrysaora* sp. and Aurelia spp. with links to climate variability. *Limnol Oceanogr* **58**(1): 235–253. DOI: https://doi.org/10.4319/lo.2013.58.1.0235

Salter, I, Kemp, AES, Lampitt, RS and **Gledhill, M** 2010 The association between biogenic and inorganic minerals and the amino acid composition of settling particles. *Limnol Oceanogr* **55**(5): 2207–2218. DOI: https://doi.org/10.4319/lo.2010.55.5.2207

Sauer, TC, Michel, J, Hayes, MO and **Aurand, DV** 1998 Hydrocarbon characterization and weathering of oiled intertidal sediments along the Saudi Arabian Coast two years after the Gulf War oil spill. *Environ Int* **24**(1–2): 43–60. DOI: https://doi.org/10.1016/S0160-4120(97)00120-7

Schiller, RV and **Kourafalou, VH** 2014 Loop Current impact on the transport of Mississippi River waters. *J Coast Res* **298**: 1287–1306. DOI: https://doi.org/10.2112/JCOASTRES-D-13-00025.1

Schiller, RV, Kourafalou, VH, Hogan, P and **Walker, ND** 2011 The dynamics of the Mississippi River plume: Impact of topography, wind and offshore forcing on the fate of plume waters. *J Geophys Res* **116**(C6): C06029. DOI: https://doi.org/10.1029/2010JC006883

Schneider, B, Schlitzer, R, Fischer, G and **Nöthig, E-M** 2003 Depth-dependent elemental compositions of particulate organic matter (POM) in the ocean. *Global Biogeochem Cycles* **17**(2): 1032. DOI: https://doi.org/10.1029/2002GB001871

Shipe, RF and **Brzezinski, MA** 2001 A time series study of silica production and flux in an eastern boundary region: Santa Barbara Basin, California. *Global Biogeochem Cycles* **15**(2): 517–531. DOI: https://doi.org/10.1029/2000GB001297

Shipe, RF and **Brzezinski, MA** 2003 Siliceous plankton dominate primary and new productivity during the onset of El Niño conditions in the Santa Barbara Basin, California. *J Mar Syst* **42**(3–4): 127–143. DOI: https://doi.org/10.1016/S0924-7963(03)00071-X

Siegel, DA and **Deuser, WG** 1997 Trajectories of sinking particles in the Sargasso Sea: modeling of statistical funnels above deep-ocean sediment traps. *Deep Sea Res Part I Oceanogr Res Pap* **44**(9–10): 1519–1541. DOI: https://doi.org/10.1016/S0967-0637(97)00028-9

Smith, SR and **Jacobs, GA** 2005 Seasonal circulation fields in the northern Gulf of Mexico calculated by assimilating current meter, shipboard ADCP, and drifter data simultaneously with the shallow water equations. *Cont Shelf Res* **25**(2): 157–183. DOI: https://doi.org/10.1016/j.csr.2004.09.010

Stout, SA, Rouhani, S, Liu, B, Oehrig, J, Ricker, RW, et al. 2017 Assessing the footprint and volume of oil deposited in deep-sea sediments following the Deepwater Horizon oil spill. *Mar Pollut Bull* **114**(1): 327–342. DOI: https://doi.org/10.1016/j.marpolbul.2016.09.046

Stuiver, M and **Polach, HA** 1977 Discussion Reporting of ^{14}C Data. *Radiocarbon* **19**(3): 355–363. DOI: https://doi.org/10.1017/S0033822200003672

Sturges, W and **Leben, R** 2000 Frequency of ring separations from the Loop Current in the Gulf of Mexico: A revised estimate. *J Phys Oceanogr* **30**(7): 1814–1819. DOI: https://doi.org/10.1175/1520-0485(2000)030<1814:FORSFT>2.0.CO;2

Thorne, C, Harmar, O, Watson, C and **Clifford, N** 2008 Current and historical sediment loads in the Lower Mississippi River., in press where in press?. Available at: http://oai.dtic.mil/oai/oai?verb=getRecord&metadataPrefix=html&identifier=ADA486343 Accessed 2017 Feb 20.

Tseng, C-M 2005 A unique seasonal pattern in phytoplankton biomass in low-latitude waters in the South China Sea. *Geophys Res Lett* **32**(8): L08608. DOI: https://doi.org/10.1029/2004GL022111

Tsunogai, S 1987 Train-passengers model as an oceanic removal mechanism of chemical elements in seawater. *Chikyu Kagaku (Geochemistry)*, in press. Available at: https://scholar.google.com/scholar?hl=en&q=%22Train-passengers+model%22+as+an+oceanic+removal+mechanism+of+chemical+elements+in+seawater&btnG=&as_sdt=1%2C5&as_sdtp=. Accessed 2017 Mar 20.

Turner, JT 2002 Zooplankton fecal pellets, marine snow and sinking phytoplankton blooms. *Aquat Microb Ecol* **27**: 57–102. DOI: https://doi.org/10.3354/ame027057

Turner, RE, Rabalais, NN and **Justic, D** 2008 Gulf of Mexico hypoxia: Alternate states and a legacy. *Environ Sci Technol* **42**(7): 2323–2327. DOI: https://doi.org/10.1021/es071617k

Valentine, DL, Fisher, GB, Bagby, SC, Nelson, RK and **Reddy, CM,** et al. 2014 Fallout plume of submerged oil from Deepwater Horizon. *Proc Natl Acad Sci U S A* **111**(45): 15906–11. DOI: https://doi.org/10.1073/pnas.1414873111

Van Metre, PC, Frey, JW, Musgrove, M, Nakagaki, N, Qi, S, et al. 2016 High nitrate concentrations in some midwest United States streams in 2013 after the 2012 drought. *J Environ Qual* **45**(5): 1696. DOI: https://doi.org/10.2134/jeq2015.12.0591

Vidal, VMV, Vidal, FV and **Pérez-Molero, JM** 1992 Collision of a loop current anticyclonic ring against the continental shelf slope of the western Gulf of Mexico. *J Geophys Res* **97**(C2): 2155. DOI: https://doi.org/10.1029/91JC00486

Villa-Alfageme, M, de Soto, FC, Ceballos, E, Giering, SLC, Le Moigne, FAC, et al. 2016 Geographical, seasonal, and depth variation in sinking particle speeds in the North Atlantic. *Geophys Res Lett* **43**(16): 8609–8616. DOI: https://doi.org/10.1002/2016GL069233

Vogel, JS, Southon, JR, Nelson, DE and **Brown, TA** 1984 Performance of catalytically condensed carbon for use in accelerator mass spectrometry. *Nucl Instruments Methods Phys Res Sect B Beam Interact*

with Mater Atoms **5**(2): 289–293. DOI: https://doi.org/10.1016/0168-583X(84)90529-9

Volkman, JK, Barrett, SM, Blackburn, SI, Mansour, MP, Sikes, EL, et al. 1998 Microalgal biomarkers: A review of recent research developments. *Org Geochem* **29**(5): 1163–1179. DOI: https://doi.org/10.1016/S0146-6380(98)00062-X

Walker, ND 1996 Satellite assessment of Mississippi River plume variability: Causes and predictability. *Remote Sens Environ* **58**(1): 21–35. DOI: https://doi.org/10.1016/0034-4257(95)00259-6

Walker, ND, Wiseman, WJ, Rouse, LJ and **Babin, A** 2005 Effects of river discharge, wind stress, and slope eddies on circulation and the satellite-observed structure of the Mississippi River plume. *J Coast Res* **216**: 1228–1244. DOI: https://doi.org/10.2112/04-0347.1

Wang, HB and **Zhang, YJ** 2014 Mechanisms of interaction between polycyclic aromatic hydrocarbons and dissolved organic matters. *J Environ Sci Heal Part A* **49**(1): 78–84. Taylor & Francis Group. DOI: https://doi.org/10.1080/10934529.2013.824311

Yan, B, Passow, U, Chanton, JP, Nöthig, E-M, Asper, V, et al. 2016 Sustained deposition of contaminants from the Deepwater Horizon spill. *Proc Natl Acad Sci* **113**(24): E3332–E3340. DOI: https://doi.org/10.1073/pnas.1513156113

How to cite this article: Giering, SLC, Yan, B, Sweet, J, Asper, V, Diercks, A, Chanton, JP, Pitiranggon, M and Passow, U 2018 The ecosystem baseline for particle flux in the Northern Gulf of Mexico. *Elem Sci Anth,* 6: 6. DOI: https://doi.org/10.1525/elementa.264

Domain Editor-in-Chief: Jody W. Deming, University of Washington, US

Associate Editor: Laurenz Thomsen, Jacobs University Bremen, DE

Knowledge Domain: Ocean Science

Part of an *Elementa* Special Feature: Impacts of natural versus anthropogenic oil inputs on the Gulf of Mexico ecosystem

Submitted: 31 May 2017 **Accepted:** 07 November 2017 **Published:** 25 January 2018

ELEMENTA Science of the Anthropocene

Elem Sci Anth is a peer-reviewed open access journal published by University of California Press.

OPEN ACCESS